

Article

Sedimentation and Erosion Patterns of the Lena River Anabranching Channel

Sergey Chalov ^{1,2,*} and Kristina Prokopeva ¹¹ Faculty of Geography, Lomonosov Moscow State University, 119991 Moscow, Russia² Institute of Ecology and Environment, Kazan Federal University, 4200097 Kazan, Russia

* Correspondence: srchalov@geogr.msu.ru

Abstract: Lena River is one of the largest “pristine” undammed river systems in the World. In the middle and low (including delta) 1500 km course of the Lena main stem river forms complex anabranching patterns which are affected by continuous permafrost, degradation of the frozen ground and changes in vegetation (taiga and tundra). This study provides a high-resolution assessment of sediment behavior along this reach. Comprehensive hydrological field studies along the anabranching channel located in the middle, low and delta courses of the Lena River were performed from 2016 to 2022 including acoustic Doppler current profiler (ADCP) discharge measurements and sediment transport estimates by gravimetric analyses of sediment concentration data and surrogate measurements (optical by turbidity meters and acoustic by ADCP techniques). These data were used to construct regional relationships between suspended sediment concentrations (SSC, mg/L), turbidity (*T*, NTU) and backscatter intensity (*BI*, dB) values applicable for the conditions of the Lena River. Further, field data sets were used to calibrate the seasonal relationships between Landsat reflectance intensities and field surface sediment concentration data. Robust empirical models were derived between the field surface sediment concentration and surface reflectance data for various hydrological seasons. Based on the integration of in situ monitoring and remote sensing data we revealed significant discrepancies in the spatial and seasonal patterns of the suspended sediment transport between various anabranching reaches of the river system. In the middle course of the Lena River, due to inundation of vegetated banks and islands, a downward decrease in sediment concentrations is observed along the anabranching channel during peak flows. Bed and lateral scour during low water seasons effects average increase in sediment load along the anabranching channels, even though a significant (up to 30%) decline in SSC occurs within the particular reaches of the main channel. Deposition patterns are typical for the secondary channels. The anabranching channel that was influenced by the largest tributaries (Aldan and Viluy) is characterized by the sediment plumes which dominate the spatial and temporal sediment distribution. Finally, in the distributary system of the Lena delta, sediment transport is mostly increased downwards, predominantly under higher discharges and along main distributary channels due to permafrost-dominated bank degradation.

Citation: Chalov, S.; Prokopeva, K. Sedimentation and Erosion Patterns within an Anabranching Lena River Channel. *Water* **2022**, *14*, 3845. <https://doi.org/10.3390/w14233845>

Academic Editor: Maria Mimikou

Received: 12 October 2022

Accepted: 22 November 2022

Published: 26 November 2022

Publisher’s Note: MDPI stays neutral with regard to jurisdictional claims in published maps and institutional affiliations.

Keywords: suspended sediment concentration; turbidity; ADCP; sediment budget; remote sensing; anabranching channel; flow distribution



Copyright: © 2022 by the authors. Licensee MDPI, Basel, Switzerland. This article is an open access article distributed under the terms and conditions of the Creative Commons Attribution (CC BY) license (<https://creativecommons.org/licenses/by/4.0/>).

1. Introduction

The evolution of large Eurasian fluvial systems since the end of the 19th century has been determined, according to recent studies, by changes that have affected the drainage basins, notably climate changes at the end of the Little Ice Age, agricultural practices, and successive phases of channel management involving embankments and dams [1,2]. However, the respective roles of these various control factors in modifying water and sediment budget along the downstream reaches have still not been identified and compared. Due

to complicated impacts of the anabranching channel pattern, inputs from tributaries (some of which are among the largest rivers on Earth), existence of huge and complex floodplains or in some case of artificial straightening of the channels and intensive changes in channel processes, a number of gaps remain in our knowledge of erosion and deposition, hydrophysical and ecological functioning and the evolution of the channel–floodplain system of the largest rivers of Eurasia [3–5]. Knowledge on the sediment transport of these rivers mainly relies on a very limited number of gauging stations, most of which are downstream. The undammed rivers in this regard are even less studied mostly due to their location in the remote northern territories of Russian Siberia [3,6–9]. Here, few rivers represent a reference for the natural state of fluvial processes and sediment transport, and the largest is the Lena which its main stem is unregulated and its total volume of the regulated river runoff in the tributaries is less than 3% of the total flow.

In recent decades, the Lena River system was subject to a variety of studies investigating different aspects of the hydrological as well as the geomorphological system components [5,10,11], particular along Lena’s delta [12–14]. As far as degradation of the frozen ground has been shown to be the main cause of the marked increase in water discharge [15–17], the links between change hydrology, fluvial processes and sediment transport are of particular interest. Some studies have identified how the aggradation patterns during floodplain inundation and fluvial erosion patterns have a huge effect on the sediment transport along the anabranching channel reaches [2]. Moreover, bank erosion due to complex ice-triggered abrasion processes represent effective sediment sources, especially in melting periods [14,18]. At the Lena River the recent channel changes have proven that the global change deeply impacts the periglacial river [19]. Under the dominant role of thermal erosion in bank retreat over sections of the anabranching fluvial system [20], the Lena River offers an opportunity to investigate the impacts of ongoing re-adjustment of the channel form to sediment transport.

Considering the notable shifts in hydromorphology along the middle and low courses of the river, we aimed to understand the continuum in sediment transport features along the river main stem. For that, we aimed at combining in situ and remote sensing techniques which can support investigation at much broader spatial and temporal scales than previously possible for the largest rivers. In situ measurements relied on gravimetric and surrogate measurements based on optical and acoustic principles. The application of surrogate measurements for the extended territory significantly enhances the in situ observations, but requires specific regional calibration curves for each drainage and stream [21]. Among the most applicable approaches is the turbidity (T). T is a unit of the degree of light scattering through a water column containing suspended organic (e.g., algae) and inorganic particles. Light scattering increases with a greater concentration of suspended particles. Turbidity is commonly measured in nephelometric turbidity units (NTU). Another promising tool is the acoustic technologies which are based on commercial acoustic Doppler current profilers (ADCPs), recognized as potential tools for the quantification of sediment transport in natural streams using echo intensity levels as a measure of acoustic backscattering strength (backscatter intensity, BI). The remote sensing data also provides a quantitative value of suspended sediment loads through earth observation data [22–29] and relies on surface reflectance data (reflectance coefficient, ρ).

Altogether, a combination of these approaches is an efficient tool for identifying long-term sediment concentration patterns over extended river reaches of such remote and poorly monitored rivers as Lena. The present study was based on field measurements and the application of remote sensing approaches to study spatio-temporal variation of suspended sediment transport. As far as all of the mentioned approaches (T , BI and ρ) have never been used in investigating the Lena River, we selected three case study areas located in the middle and low course of the Lena River representing various types of anabranching permafrost-affected channel patterns to develop and further apply a set of in situ and remote sensing tools to study the sedimentation patterns of the Lena River. The paper focuses on three main objectives:

1. To construct a set of regional empirical models between the surface sediment concentration and T , BI and ρ ;
2. Examine the variability in surface sediment distribution revealed by satellite images and total sediment budget by ADCP along the Lena anabranching channel;
3. Provide a comparative study of the erosion and sedimentation patterns between various parts of the river system with a particular focus on the impacts of the thermal erosion processes on suspended sediment transport.

2. Study Area

The Lena River is the largest Arctic River, originating near Lake Baikal entering into the Arctic Ocean via the Laptev Sea, crosses East Siberia from south to north, and has a length of 4400 km. The Lena basin extends throughout almost all of East Siberia (Yakutia) with an area of 2.5×10^6 km². The Lena River contributes 524 km³ of freshwater per year, or about 15% of the total freshwater flow into the Arctic Ocean [30,31] (Figure 1). Almost the entire (approximately 78–93%) basin is located within the permafrost zone. Various types of permafrost exist in the Lena basin, including sporadic or isolated permafrost in the source regions, and discontinuous or continuous permafrost in the downstream regions [32]. Unfrozen sediments (taliks) underlie the main channel of the Lena River due to the warming of the large water mass [5]. In the middle and lower reaches of the Lena River, the talik occupies only 10–15% of the total area of the channel [33]. It is in this narrow strip in the core zone of the interflow that the most intense changes are localized, without capturing the entire channel as a whole [34]. River runoff in the study area is mainly formed during the warm period from May to July (about 75–95%). River floods start in the southern part of the basin in late April to early May and in the northern part in late May to early June. The flood duration on most of the rivers lasts for 35–40 days. About 20–30% of the spring flood is formed due to liquid precipitation. A distinct winter low-flow period lasts for roughly 200 days on average, early November till early May, with a long-term mean discharge of 1520 m³s⁻¹. Air temperatures frequently reach the -50 °C mark during the winter season, ice thickness is on average 0.32 m, and it frequently exceeds 2.0 m in secondary branches. Rapidly, normally within 10 to 15 days, streamflow increases due to melting.

In the upper valley the Lena River incises into the Trans-Baikal Highlands and the Archean Aldan Shield and flows through narrow valleys with relatively steep gradients. In the middle and low valley, the river drains the plateaus of the Siberian Platform and forms few extended reaches of anabranching channels between Pokrovsk and Zhigansk and then into the main downstream along the Lena delta. The large islands (1–5 km in length in the middle course and up to 50 km in the delta) are the predominant feature of the fluvial landscape, but the morphology and dynamics of these islands are different due to gradients in the permafrost [32] and vegetation (from taiga forests to tundra), as well as distinctions in their origin. In particular, islands of the middle course are formed by alluvial processes and consist of alluvium; the islands of the delta are mainly composed of a sandy material and alluvial peat. Sandy sequences covered by the so-called ice complex (IC) form on the third terrace of islands. Ice complex are permafrost areas which usually consist of fine-grained loess-like sediments within organic-rich to peaty formations. They have a high content of segregated ice and polygonal ice wedges several meters in height and width [35]. The particular modes of fluvial processes within this anabranching channel are formed under the impact of the largest tributaries—Aldan and Viluy Rivers.

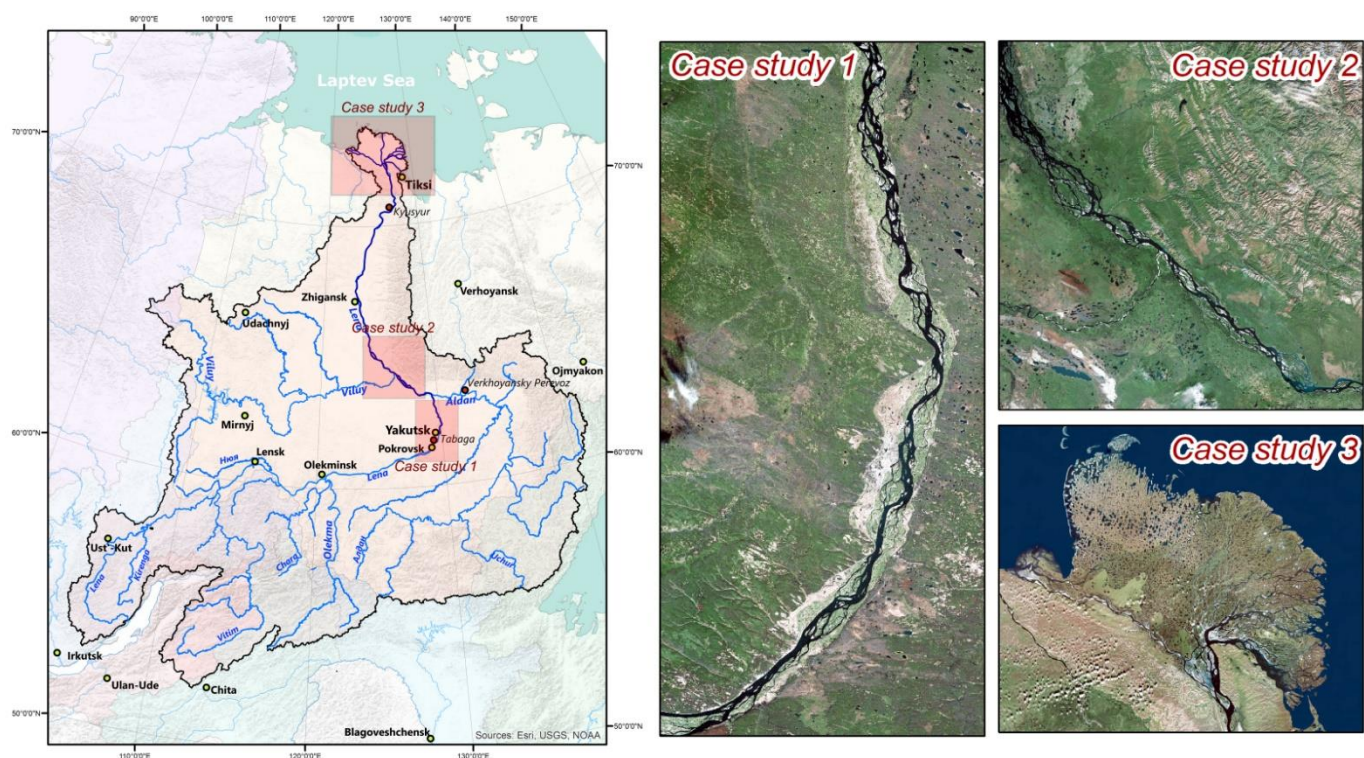


Figure 1. Lena River basin and the locations of case studies.

Our study was conducted at three main sections of the Lena River. Case study 1 (Figure 1) was located in the middle reach of the Lena River, between Pokrovsk and the confluence of the Lena and Aldan Rivers. Upstream of Yakutsk, the floodplain widens, and the river develops a complex branching of the river channel, numerous channels surround the largest sand bars and forested islands. The width of the channel with islands can reach 10 km and the width of the river valley is up to 25 km. The river's longitudinal gradient sharply reduces, and the sediment observed on the bars consists of medium and fine sands [10]. The mean annual water discharge recorded at the Tabaga gauging station located here is around $8\,300\text{ m}^3\text{ s}^{-1}$ for the last decade. This is typical of an anabranching pattern in the middle course of the Lena River. Alluvial vegetation on the Lena islands here is very homogeneous and is dominated by willows.

Case study reach 2 (Figure 1) is the Lena channel from Aldan River to Zhigansk. Two main tributaries flow into the Lena River in this section: Aldan (right) and Viluy (left). The Aldan River is a higher energy system, transporting a larger fraction of sediment and finer gravel up to the junction with the main river. Downstream of the Viluy River junction, the Lena turns north and keeps this direction up to the Laptev Sea. The floodplain is asymmetric, the right side of the river is flanked by the Verkhoyansky Mountains, while on the left side, the floodplain can be more than 20 km wide with numerous complex anabranching and unstable channels, swamps, and thermokarst lakes.

The most downstream anabranching channel (case study 3) is located within the distributary delta system of the Lena River. With $16,500\text{ m}^3\text{ s}^{-1}$ average annual discharge at Kyusyur (gauging station located at the entrance of the Lena delta), here the river can be defined as a “mega-river” [36]. The Lena River delta is the largest Arctic delta with an area of about $29,630\text{ km}^2$ [12], with more than 6000 branches with a total length of 14,600 km [37]. Here, four main distributaries represent the main sectors of the channel structure: the largest is the Trofimovskaya branch; the second-largest branch by water discharge is the Bykovskaya branch that turns sharply to the east after Sardakh Island and flows into the Buor Khaya Gulf. The third and fourth-largest distributaries are the Olenekskaya branch which flows west into the Kuba Gulf and the Tumatskaya branch which flows north into

the Laptev Sea. The origin of this area is particularly different from the anabranching channel of the middle course: delta terraces were not formed as deposits made by the flooding river, i.e., river terraces [12]; rather, they were formed by Laptev sea-level fluctuations over a long period of time and thus the surface is significantly higher, hampering possible submerging.

3. Materials and Methods

3.1. Field Observations

Acoustic Doppler current profiler (ADCP) measurements along case study 1 were performed from 25 June to 2 July 2020, 23 to 25 September 2021 and 10–20 June 2022 at over 30 branches of the Yakutsk anabranching reach. The measurements were further processed to calculate eight total river discharges as the sum of particular branches in the valley cross-section (Figure 2a). The ADCP measurements within case study 2 were performed from 3 to 10 July 2020 and from 3 to 6 July 2021 at 17 cross-sections within the most extended anabranching reach below the confluence of the Viluy River (Saham anabranching reach) (Figure 2b). ADCP measurements in the Lena delta were conducted between 10 and 16 August 2022 and included 25 ADCP discharge measurements in the Bykovskaya, Bulkurskaya, Olenekskaya, Tumatskaya, Arinskaya branches and in the main channel (Figure 2c).

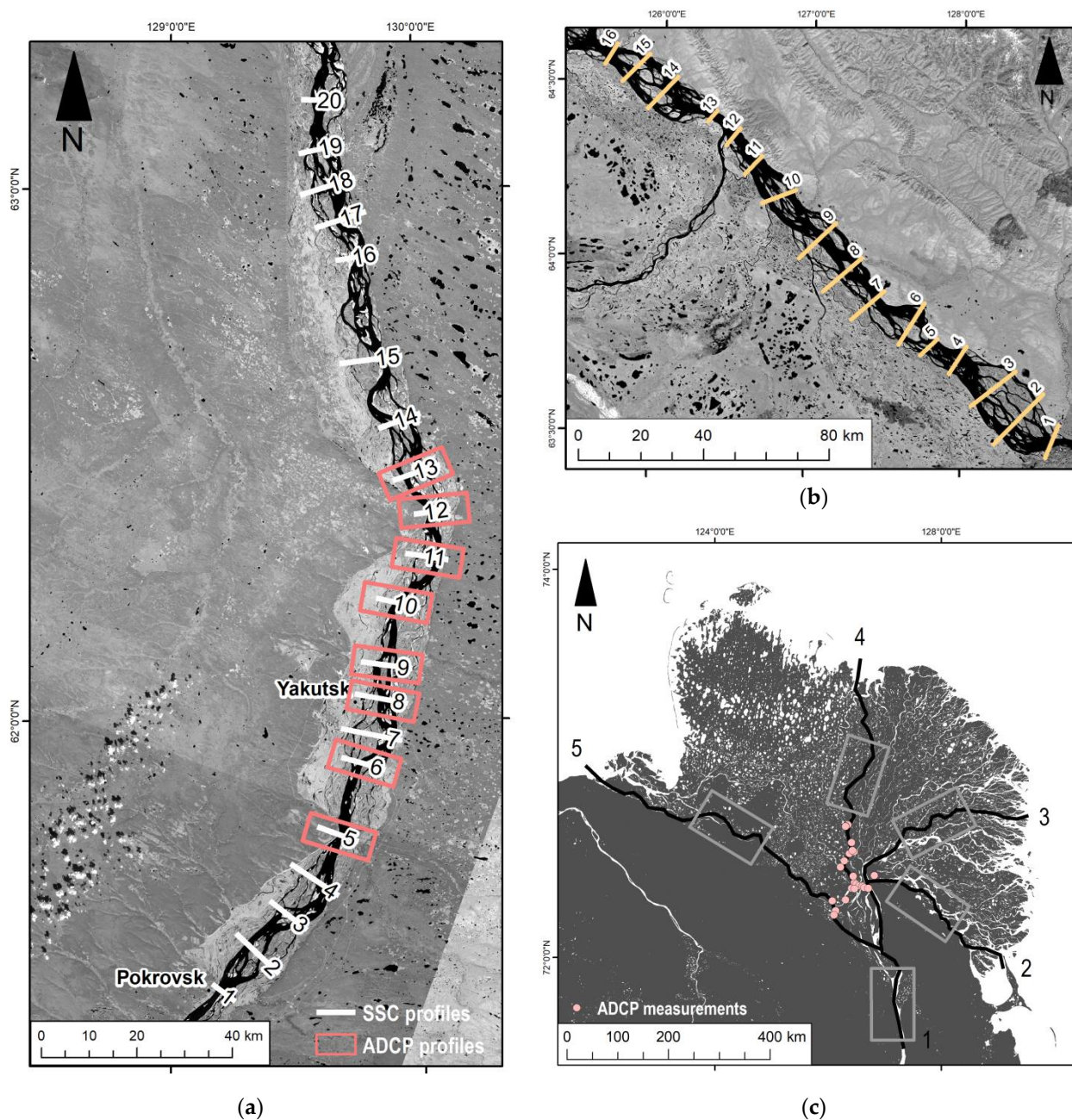


Figure 2. Schematic map of the sections and profiles, where SSC changes were calculated: (a) numbers represent the profile locations of the SSC sections in case study 1; (b) numbers represent the profile locations of the SSC sections in case study 2; (c) numbers represent channels in the Lena River delta (case study 3): 1—main channel; 2—Bykovskaya, 3—Trofimovskaya, 4—Tumatskaya, 5—Olenekskaya branches; grey boxes are polygons for calculating average sediment concentrations.

The main part of the field data used in this study was related to gravimetric SSC (mg/L) and water turbidity (NTU) measurements (Table 1). Water samples were pumped out with a filterless, submersible 12 V pumps from three layers: surface, mid-section, and near-bottom to account for the vertical distribution of the suspended sediment. For SSC determination water samples were filtered through pre-weighed and pre-dried (at 105 °C for two hours) membrane filters (pore size 0.45 µm) from the “Millipore” filtration system (Germany manufacturer). The filter samples were then oven-dried (at 105 °C for two hours) and re-weighed to determine suspended sediment concentrations. The mass of dry sediment was determined by gravitational differences. The SSC was deduced from the measured mass of the dry sediment and the water sample volume:

$$SSC = \frac{m_2 - m_1}{V} \quad (1)$$

where m_2 is the mass of the filter and dried residue (mg), m_1 is the mass of the clean filter (mg), and V is the volume of the filtered water sample (L). The mass of the membrane filter and the wet sediment were measured with an accuracy of less than 0.001 g.

Grain-size analysis of the suspended sediments was conducted with the Laser Particle Sizer Fritsch Analysette 22 (Germany manufacturer). The average 50% (D_{50} , μm) was calculated for each sample using the measured grain-size distribution curves linearized to double logarithmic coordinates and interpolated. The turbidity data was obtained in NTU using a portable Hach turbidity meter (USA manufacturer). The 2100 P portable turbidimeter combines microprocessor-controlled operations and Hach's patented ratio optics. By providing a direct digital readout in nephelometric turbidity units (NTUs), the need for calculations or interpolation of calibration charts is completely eliminated. We took three water samples at each river sampling point, measured the turbidity in situ, and calculated the mean turbidity.

Table 1. Data characteristics used in empirical SSC models of the Lena River.

Data Type	Case Study	Date of Sampling	Samples	Water Discharges Range, m^3s^{-1}	D50, μm		
					Average	Max	Min
Turbidity (NTU)	1	20–29 June and 8–10 July 2016	82	12,200–26,400 (by Tabaga gauging station)			
	1	25 June–10 July 2020	58	14,400–25,500 (by Tabaga gauging station)	21.8	25.3	13.0
	2	27 June 2020	17	42,900 (authors measurement in Saham anabranching system)	34.7	68.0	21.7
	2	3–5 July 2021	20	19,700 (authors measurement in Saham anabranching system)	14.7	21.8	6.89
	1	20–23 September 2021	86	12,600 (authors measurement in Yakutsk anabranching system)	11.3	16.3	6.33
	1	10–19 June 2022	38	20,200–25,200 (authors measurement in Yakutsk)	25.6	64.6	16.7
	3	10–16 August 2022	22	31,300 (authors measurement in 4.7 km upper Stolb island)	15.0	18.6	10.9
Surface water samples (SSC)	1	20–28 June and 9 July 2016	39	12,400–26,400 (by Tabaga gauging station)			
	2	7 July 2020	8	16,400 (by Tabaga gauging station)	21.8	25.3	13.0
	3	13–15 August 2022	32	31,300 (authors measurement in 4.7 km upper Stolb island)	14.7	17.1	11.0
ADCP	1	25 June and 2 July 2020	8	20,300–25,500 (by Tabaga gauging station)	21.8	25.3	13.0
	1	23–25 September 2021	6	12,600 (authors measurement in Yakutsk anabranching system)	11.3	16.3	6.33
	1	10–19 June 2022	12	20,200–25,200 (authors measurement in Yakutsk anabranching system)	25.6	64.6	16.7

SSC and turbidity measurements were in many cases coupled with simultaneous discharge measurements with ADCP using a Teledyne RD Instruments (TRDI) RioGrande WorkHorse 600 kHz ADCP (USA manufacturer) unit mounted on a moving boat. For each

sample at a depth profile, the boat was repositioned to its original location and sampling was performed while drifting at the river water velocity. These measurements were used to calibrate the relationship between the backscatter and suspended sediment concentrations using the power-law least-squares fitting between the raw backscatter values (BI) and the measured suspended sediment concentration (SSC) for the specific rivers and hydrological seasons [38]. For this purpose, only profiles with a sufficient amount of simultaneous SSC gravimetric and ADCP-based BI measurements carried out under constant discharge conditions were considered. Further, an ASET software package for calibrating and processing TRDI ADCP data to compute the suspended sediment load W_R was used to count suspended sediment loads measured by ADCP [39].

Particular in situ SSC measurements were collected concurrently during field campaigns in the middle of the Lena River from Yakutsk to the Viluy River on 9 July 2016 (21 measurements corresponding to the flood water period) and from 20 June to 9 July 2020 (26 measurements corresponding to the end of the flood water period) (Figure 3a,b) and were used for the calibration of Landsat images from 9 July 2016 and from 20 June and 9 July 2020. We also used SSC data during field campaigns in the Lena River delta from 13 to 15 August 2022 (32 measurements) and the available satellite images for these dates (16 August 2022) (Figure 3c). Surface water samples were collected at a depth of 0–0.5 m using a pump water sampler, preserved in 5 L clean bottles at various locations along the river channel.

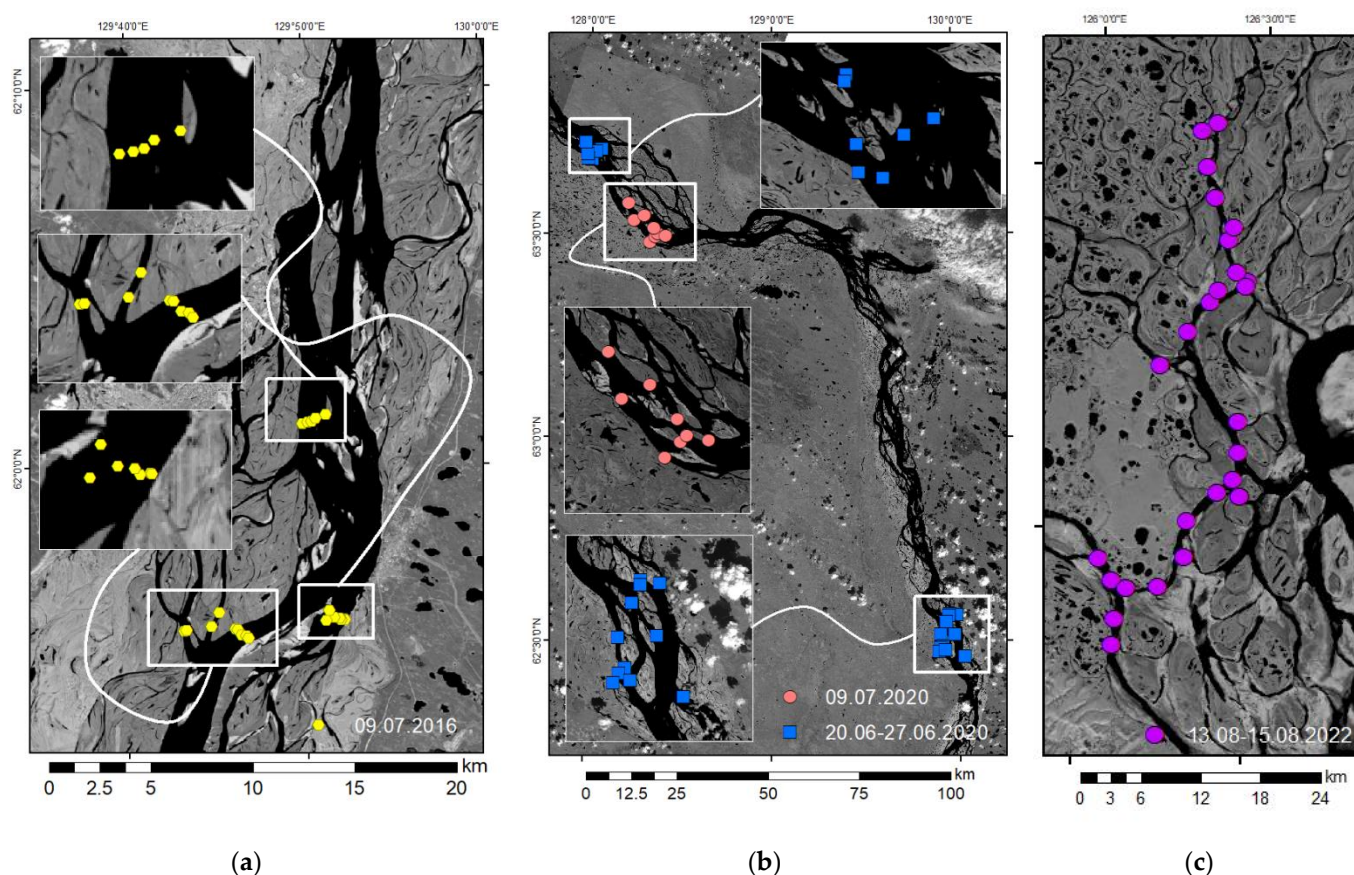


Figure 3. Locations of the field measurements of the SSC in the middle reach of the Lena River: 9 July 2016 (a), 20 June till 9 July 2020 (b) and in the Lena River delta: 13–15 August 2022 (c) used for regression model construction.

3.2. Processing Satellite Images Data

The estimation of suspended sediment concentration (SSC) from remote sensing imaging has been investigated since the 1970s [40]. Generally, it has shown both theoretically

and empirically that optical bands are highly correlated with SSC [41], particularly in the red wavelength range of 610–700 nm, if the SSC is within the range of 0–50 mg/L, near-infrared wavelength range of 700–1000 nm, which correlate with an SSC for higher concentrations of SSC, but become uncorrelated for lower values and band combinations (NIR used with a ratio of optical bands: usually the red band but sometimes the green band) particularly with high SSC values [42]. The type of relationships between SSC and reflectance can change depending on the presence of other optical materials, such as algae or dissolved organic matter. There is generally a linear relationship in optical bands (blue, green and red) and an exponential relationship for higher SSCs [43].

We used high-resolution satellite imaging from the Landsat satellite system to track variations in SSC. The Landsat satellite system is freely available and provides 30 m spatial resolution with a respective 16-day cycle sufficient to reconstruct surface sediment concentrations in the main channel and branches of the Lena River during the long-term period. Utilizing all four Landsat systems allowed for continuous monitoring of the seasonal variations and patterns.

Landsat Collection-1 Level-1 data products were downloaded from the USGS Earth Explorer website from 1992 to 2018 for the middle of the river and from 1999 to 2022 for the Lena delta to create the Landsat database. Remotely sensed data used for this study were Landsat 4 and 5 Thematic Mapper (TM), Landsat 7 Enhanced Thematic Mapper Plus (ETM+), and Landsat 8 Operational Land Imager (OLI). The study relied on 150 images: 90 were used to derive long-term SSC in case study 1 and 2 (middle reach of the Lena River), 50 images for case study 3 (Lena River delta), and 10 Landsat 8 images were used to calibrate and validate the “reflectance–SSC” model. Landsat images were first radiometrically calibrated and atmospherically corrected by the QUAC method (Quick atmospheric correction) [44]. The digital number (*DN*) recorded by a satellite imaging system depends on sensors (spectral bands, gains, offsets), sun elevation (time of year, latitude, typically not time of day because most current satellite images are collected at around the same time of day—10:40 am local time for Landsat), atmosphere (conditions-scattering/absorption), topography (slope and aspect). The conversions from *DN* to absolute units provide a basis for standardized comparison of data in a single scene or between images acquired on different dates or by different sensors excluding sun and atmosphere influence [45]. Calibrated digital numbers (*DN*s) to absolute units of at-sensor spectral radiance, top-of-atmosphere (TOA) reflectance were converted using equations and rescaling factors for the Multispectral Scanner (MSS), Thematic Mapper (TM), Enhanced Thematic Mapper Plus (ETM+), and Advanced Land Imager (ALI) sensors for the Multispectral Scanner (MSS), Thematic Mapper (TM), Enhanced Thematic Mapper Plus (ETM+), and Advanced Land Imager (ALI) sensors [46].

The Landsat data used in this study was atmospherically corrected using the DOS (dark object subtraction) method. DOS models are used to remove the effects of atmospheric scattering from images by subtracting the darkest pixel value that represents a background signature from each band. This value can be the band minimum, an average based upon a region of interest (ROI), or a fixed value [44,47]. A major advantage over more rigorous radiative transfer models is that surface and/or atmospheric field data collected at the time of overflight are not needed. Therefore, entirely image-based models, such as DOS, can be applied to retrospective images as well as images of areas that are not easily accessible [47].

We reduced a collection of images “to the common denominator”, which is called the “reference” image for relative atmospheric correction. The “reference” was an image of the middle reach of the Lena River from 7 July 2016 (path = 121, raw = 017) with a “dark object” value of 0.0156. The remaining images of the series were reduced to first reference values. On the series of images taken on different dates, dark objects have the same brightness and any differences in the images are due to the influence of the atmosphere. In case of the research reported here, the “dark object” was a clean thermokarst and the floodplain

lakes were used as a “dark object”. Then, each satellite image calculated the differences between the reflectance coefficients of “dark objects”.

3.3. Sedimentation Patterns Analyses

The processing of in situ and remote sensing data aimed to understand the erosion and sedimentation patterns over the case study reaches along the middle and lower course of the Lena River using three different approaches.

The first approach was based on the measured suspended sediment load W_{Rs} (kg s^{-1}) by ADCP, processed according to [38]. Using ADCP sediment load measurements we estimated daily sediment loads as $W_R = 86,400W_{Rs}$, which was used to calculate the sediment budget between adjacent cross-sections:

$$\Delta W_R = W_{Rdown} - (W_{Rup} + W_{Rtrib}) \quad (2)$$

where W_{Rdown} and W_{Rup} are the sediment loads at the downstream and upstream profiles of a considered reach crossing river valley, respectively, and W_{Rtrib} is the sediment load from tributaries along the reach. In the case of the anabranching channel, each W_R value includes the sum of the sediment load at each branch within a particular valley cross-section. $\Delta W_R > 0$ corresponds to the erosion patterns, whereas $\Delta W_R < 0$ evidence deposition–aggradation patterns.

The second approach was based on the analyses of surface sediment concentration maps generated by applying the retrieved empirical models $SSC = f(\rho)$ from available Landsat 5, Landsat 7, Landsat 8 images for each of the case studies. We collected 62 cloud-free and open-water satellite images from all the analyzed sensors for the ice-free period (June–September) from 1992 to 2018, which covered a high range of water discharge variation (discharges from $4760 \text{ m}^3\text{s}^{-1}$ to $36,300 \text{ m}^3\text{s}^{-1}$ by Tabaga gauging station) for the channel reach between Pokrovsk and the Aldan River (case study 1). For case study 2 of the Lena River (from the Aldan River to Zhigansk) we collected 30 images from 1999 to 2020. Water discharges were calculated using data from the Tabaga gauging station on the Lena River (185 km from the mouth of the Aldan River) and the Verkhoyansky Perevoz gauging station on the Aldan River (140 km from the mouth of the Aldan River). During this period water discharges varied at the Tabaga station from $6850 \text{ m}^3\text{s}^{-1}$ to $31,400 \text{ m}^3\text{s}^{-1}$, at the Verkhoyansky station from $3920 \text{ m}^3\text{s}^{-1}$ to $26,000 \text{ m}^3\text{s}^{-1}$. A total of 47 images from the 1999–2021 period were used to determine SSC changes along the Lena River delta. The third part of the data set covered water discharges from $17,000 \text{ m}^3\text{s}^{-1}$ to $72,200 \text{ m}^3\text{s}^{-1}$ at the Kyusyur gauging station. All images were classified into two classes: water and other (including land, cloud cover/shade, sand bar and aquatic vegetation) over a wide area around each station. SSC maps were generated for the water class. Most of the operations, such as digital numbers to reflectance calculation and water mask creation, were performed in ArcGIS software. Tools for radiometric and atmospheric correction were performed in the QGIS software using a semi-automatic classification plugin, which provided calibration coefficients for all the Landsat sensors. All available images were transformed into the generated surface sediment concentration maps.

The third approach was based on surface sediment concentration SSC profiles. For the case study area 1, we selected 20 cross-sections to calculate the longitudinal change in SSC (Figure 2a). Similarly, 16 cross-sections were taken along case study 2 between Aldan and Viluy confluences (Figure 2b). Between each of these cross-sections the SSC change (ΔS_0) was calculated on the basis of the difference between SSC at the upstream (SSC_1) and downstream (SSC_2) locations:

$$\Delta S_0 = SSC_2 - SSC_1 \quad (3)$$

Values for SSC_1 and SSC_2 were estimated as an average for every cross-section. Relative sediment changes ΔS (%) were calculated as:

$$\Delta S = \Delta S_0 / SSC_1 \quad (4)$$

For case study 3 (Figure 2c) each of Equations (3) and (4) were applied for different distributary river sections: the main channel and four branches: Bykovskaya, Trofimovskaya, Tumatskaya, and Olenekskaya channels. Three possible ratios between the sediment input and output were analyzed: $SSC_2 > SSC_1$, $SSC_2 < SSC_1$, and $SSC_2 \approx SSC_1$, which corresponded to either erosional ($\Delta S > 0$) or deposition ($\Delta S < 0$) patterns. Representative sections and profiles were selected from each study area to calculate the surface SSC changes (Figure 2).

4. Results

4.1. Set of Regional Lena River Models for SSC Determination

Based on in situ measurements and remote sensing data we constructed a set of regional empirical models between the surface sediment concentration SSC and T , BI and ρ for the Lena River (Table 2). Some of them were similar for the entire middle and lower reaches of the Lena River (T and BI), while the $\rho = f(SSC)$ generally varied between the various hydrological seasons but can also be interpolated using a single relationship.

According to the measurements in case study 1, average $D50$ decreased from 25.6 μm (flood water, 2022) to 11.3 μm (low water, 2021). In case study 2 measurements were carried out only during flood water (27 June 2020) and low water (3–4 July 2021) and the average $D50$ s decrease from 34.7 μm to 14.7 μm , respectively. The average size of all the measurements was 19.6 μm . For case study 3 we sampled during August 2022, when the average $D50$ was 15.0 μm . Additionally, we calculated the maximum and minimum of $D50$ values. Maximum values were observed in case study 2 (Saham anabranching system) during the summer expedition campaign at the end of July and the values increased to 68.0 μm . Minimum values were observed during the period of low water, e.g., September 2021 measurements, and were 6.33 μm (Table 1).

Table 2. Lena River empirical SSC models.

Parameter	Study Reach, Hydrological Season	Equation	R ²
Turbidity T , NTU	Case study 1, 2, 3	$SSC = 0.95T + 5.56$	0.81
Backscatter intensity BI , dB	Case study 1	$SSC = 0.59e^{0.382BI}$	0.57
Reflectance coefficient ρ (of the Landsat image in the red spectral band)	Case study 1, low water season	$SSC = 540\rho - 2.61$	0.91
	Case study 1,2 low water season	$SSC = 1046\rho - 13.0$	0.94
	Case study 1, spring–sum- mer flood water season	$SSC = 891\rho - 7.65$	0.82
	Case study 3, low water season	$SSC = 1470\rho - 24.7$	0.62
	Case study 1, 2, 3	$SSC = 1.42e^{86.3\rho}$	0.66

The $SSC = f(T)$ relationship was based on almost 360 simultaneous measurements over case studies 1, 2 and 3 at different seasons and yielded a good correlation between all the data. Consistently, a monotonic increase in SSC with increasing turbidity T was observed (Figure 4). The $SSC = f(BI)$ relationship was performed based on 18 measurements carried out on case study 1, which led to the following relationship ($R^2 = 0.57$).

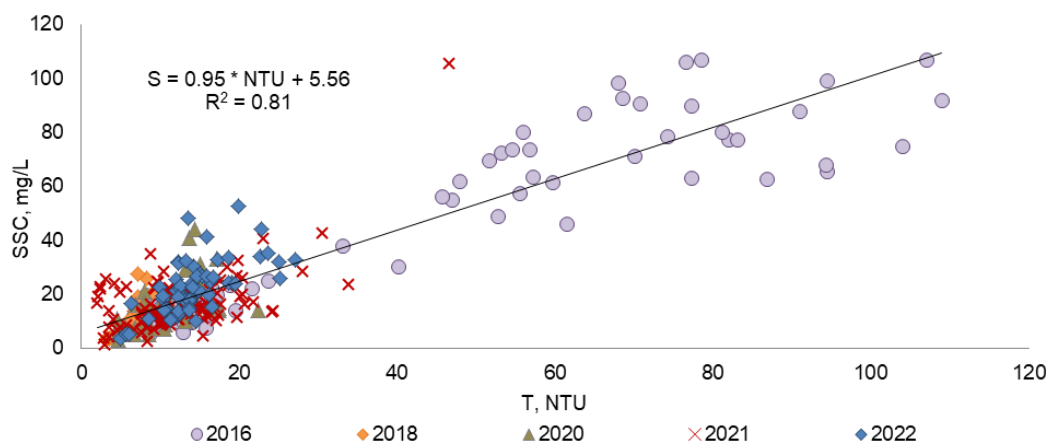


Figure 4. The $SSC = f(T)$ relationship for the middle and low courses of the Lena River. 2016-model: 82 measurements from 20 to 29 June and from 8 to 10 July 2016 (Lena River Yakutsk anabranching system). 2020-model: 58 measurements from 25 June to 10 July (Lena River from Pokrovsk to Saham anabranching system). 2021-models: 106 measurements 2 expeditions: from 3 to 5 July (Saham branching system) and from September 23 to September 25 (Yakutsk anabranching system). 2022-model: 38 measurements from 10 to 19 June (Lena River Yakutsk anabranching system) and 22 measurements from 10 to 16 August (Lena River delta).

Based on Landsat images we generated two models for different sections of the river and different phases of the water regime using in situ observations and reflectance coefficients (ρ) from the Landsat 8 remote sensing system. We selected simultaneous satellite images for two expedition data sets: according to the data from 2016 (9 July) for case study 1 and data from the period of 20 June to 28 June 2020 for case study 2 (Table 3). The calibration of the $SSC = f(\rho)$ relationship was conducted based on the combination of the SSC field data with the available Landsat images. Subsequently, “reflectance–SSC” model calibration was performed as the empirical relationship between these two parameters, plotted on a graph (Figure 5). On the total available data set we carried out statistical analyses to generate the least regression models to predict the surface sediment concentration as a function of the surface reflectance for each selected river. The equation of the approximating line presents the relationships of the image brightness of ρ and SSC. The highest accuracy was achieved using a single technique and preparation of the satellite data on the image’s brightness to eliminate radiometric and atmospheric influence.

Table 3. Descriptive statistics associated with in situ SSC and Landsat satellite images used in the study for “Reflectance–SSC” model calibration.

Path/Row	Acquisition Date	Date of Water Sampling	Sam-ples (n)	SSC, mg/L				
				Min	Max	Mean	Median	Std. Devi-ation
121/017	9 July 2016	9 July 2016	21	7.16	13.0	9.79	10.5	1.89
122/016	25 June 2020	20 – 28 June 2016	18	10.9	20.5	16.2	16.8	2.68
124/015	9 July 2020	7 July 2020 2020/07/07	8	9.91	16.4	12.2	11.5	2.40
129/009	16 August 2022	13-15 August 2022	24	3.55	22.6	13.6	14.7	4.55

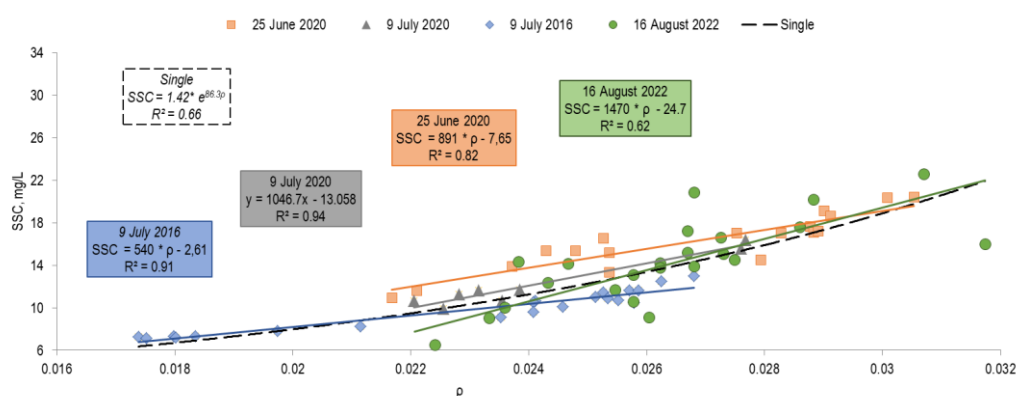


Figure 5. A regression model derived for the Lena River. SSC—suspended sediment concentration of water, ρ —the reflectance coefficient of the Landsat 8 images in the red band. The lines show the regression equation lines from Table 3.

The verification of the revealed Landsat models was performed based on the independently measured SSC data sets. The accuracy of the models was calculated using these models to satellite image; the known field observation data were not used in model calibration. For validation of the “2016-model” we used in situ measurements from the expedition in 2020 and vice versa for the “2020-model”. Applying the 2016-model to the satellite image from 25 June 2020 (field measurements on 20, 27 and 28 June 2020), the value of the mean absolute error of the modeled concentrations was approximately 1.55 mg/L. The average value of mean absolute percentage error was approximately 10%. The root means square error (1.83) was low and acceptable. However, there were also large deviations in the range of small and high values, reaching 26% (Table 4).

Table 4. Statistical comparisons between the modeled SSC retrieved from satellite data by the “2016-model” and measured in situ SSC.

Date of Water Sampling	Acquisition Date	SSC, mg/L		MAE, mg/L	MAPE, %	MSE	RMSE, mg/L
		Observed	Modeled				
20 July 2020		14.6	16.6	2.0	13.7		
20 July 2020		17.7	16.6	1.1	6.21		
20 July 2020		19.1	16.9	2.2	11.5		
20 July 2020		10.9	13.8	2.9	26.6		
20 July 2020		17.1	16.8	0.3	1.75		
20 July 2020		17	16.3	0.7	4.12		
20 July 2020		17.2	17	0.2	1.16		
20 July 2020		20.3	17.5	2.8	13.8		
20 July 2020	25 July 2020	20.4	17.6	2.8	13.7		
20 July 2020		18.6	16.8	1.8	9.68	3.37	1.83
28 July 2020		13.4	15.5	2.1	15.7		
28 July 2020		13.9	13.8	0.1	0.72		
28 July 2020		11.7	14.7	3	25.6		
28 July 2020		15.4	14.7	0.7	4.55		
28 July 2020		17	16.1	0.9	5.29		
28 July 2020		16.5	14.5	2.0	12.1		
27 July 2020		15.4	14.7	0.7	4.55		
Mean				1.55	10		

MAE—mean absolute error, MAPE—mean absolute percentage error, MSE—mean squared error, RMSE—root mean squared error.

According to the results from applying the “2020-model” to the satellite image of 9 July 2016 the mean absolute percentage error and the mean absolute error of the modeled

concentrations were 1.26 mg/L and 15%, respectively, while the root means square error by the “2020-model” was low, reaching 1.96 mg/L. However, there were also high errors in the range of the maximum and minimum concentrations due to the “2020-model” was calibrated for values within the range of 10 to 20 mg/L, while the measured values in 2016 were 7.3–13.0 mg/L. The “2020-model” showed low errors in the range of 9–13 mg/L (Table 5).

Table 5. Statistical comparisons between modeled SSC retrieved from satellite data by the “2020-model” and measured in situ SSC.

Date of Water Sampling	Acquisition Date	SSC, mg/L		MAE, mg/L	MAPE, %	MSE	RMSE, mg/L
		Observed	Modeled				
9 July 2016		10.7	11.5	0.80	7.48		
9 July 2016		10.1	10.5	0.40	3.96		
9 July 2016		9.1	9.4	0.30	3.30		
9 July 2016		12.5	11.5	1.00	8.00		
9 July 2016		10.7	10	0.70	6.54		
9 July 2016		10.5	9.9	0.60	5.71		
9 July 2016		11.5	11.2	0.30	2.61		
9 July 2016		10.9	11.3	0.40	3.67		
9 July 2016		11.0	11	0.00	0.00		
9 July 2016		7.3	4.2	3.10	42.5		
9 July 2016	9 July 2016	7.3	5.1	2.20	30.1	3.86	1.96
9 July 2016		7.3	3.5	3.80	52.1		
9 July 2016		7.2	3	4.20	58.3		
9 July 2016		7.8	5.9	1.90	24.4		
9 July 2016		8.3	6.9	1.40	16.9		
9 July 2016		7.2	4.3	2.90	40.3		
9 July 2016		13	12.3	0.70	5.38		
9 July 2016		11.6	11.6	0.00	0.00		
9 July 2016		11.6	11.8	0.20	1.72		
9 July 2016		10.5	11.7	1.20	11.4		
9 July 2016		9.6	9.9	0.30	3.13		
Mean				1.26	15.6		

MAE—mean absolute error, MAPE—mean absolute percentage error, MSE—mean squared error, RMSE—root mean squared error.

The difference in accuracy of the two models was acceptable for determining the SSC from satellite images. Higher statistical values of the “2016-model” were due to the since the satellite information was collected at the same time as the individual SSC measurements, that is, the change in water discharges did not affect in any way the changes in SSC. A completely different calibration for the “2020-model”, which was developed from satellite images from 25 June 2020 and ground-based observations, was used from 20, 27 and 28 June 2020.

4.2. Erosion and Sedimentation Patterns of the Lena River—From Pokrovsk to Aldan (Case Study 1)

The long-term estimates of the erosion and sedimentation patterns of the Lena River—from Pokrovsk to Aldan—were revealed from the Landsat images. We analyzed 62 SSC maps from 1992 to 2018 and emphasized two major types of sediment distributions: longitudinal increase (1) longitudinal decrease (2) in SSC (Figure 6). The suspended sediment load changes (according to Equations (3) and (4)) revealed from satellite images demonstrated changes in surface suspended sediment along the 200 km reach from Pokrovsk to the Aldan River. The SSC maps showed the situation under bar-full and bank-full discharges ($> 20,000 \text{ m}^3\text{s}^{-1}$, Figure 6a,b) were related to the level that submerged barren bars and the top of the water level before overbank submersion. These maps highlight the

decrease of 10–20% SSC (from 26 to 20 mg/L along the main central branch) along the 200 km reach. The picture was relatively unstable due to the impact of water diversions over the smaller branches and floodplains which can cause a very contrasting effect on the SSC.

Under the lower discharges (Figure 6c,d) a downward increase in suspended sediment concentrations occurred ($Q < 20,000 \text{ m}^3\text{s}^{-1}$). In some cases, the downward trends were not possible to detect due to sediment plumes extended under particular banks from upstream sediment sources (tributaries or eroded banks). The sediment plumes of turbid waters ($\text{SSC} > 100 \text{ mg/L}$) are mostly associated with floods. Their length along the anabranching channel can be over 100 km. This situation happened in less than 10% of the observed images, but it was typical for case study 1, as shown below.

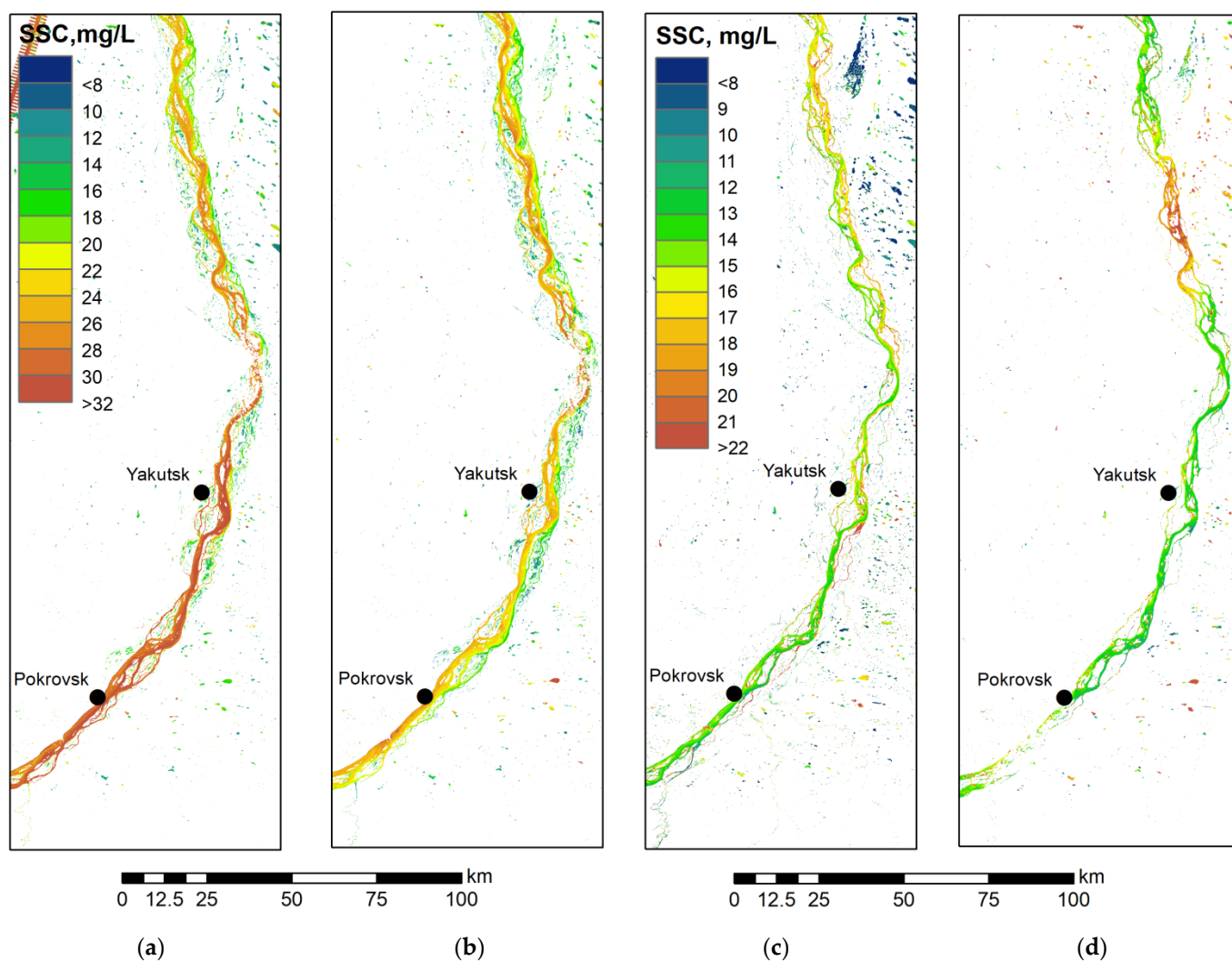


Figure 6. SSC maps for the Lena case study 1 demonstrating examples of longitudinal sediment concentration increase: (a) 15 June 2007 under a Lena discharge of $36,300 \text{ m}^3\text{s}^{-1}$; (b) 21 June 2021 under a Lena discharge of $24,200 \text{ m}^3\text{s}^{-1}$; and a decline: (c) 19 September 2013 under a water discharge of $8680 \text{ m}^3\text{s}^{-1}$; (d) 30 July 2021 under a Lena discharge of $9480 \text{ m}^3\text{s}^{-1}$.

This reach includes four relatively separate anabranching reaches located in the valley widening called Pokrovsk, Yakutsk (located near Yakutsk), Kangalas and Haityaalakhsk (Figure 7). The reaches are divided by short reaches of confined river related to their parent banks. The average data presented in the box plot demonstrates that each of these anabranching reaches was associated with a downward decrease in SSC: the higher SSCs are seen in the upper profiles of each of the reaches shifted by lower values of SSC.

The rates of longitudinal increase in the suspended sediment runoff were highest ($\Delta S_0 = 6$ mg/L) along the upstream part of the middle reaches at the site of the flow distribution and formation of a complex of floodplain anabranches. The most intensive decrease in surface sediment concentration from 32–34 mg/L to 26–28 mg/L occurred along the Yakutsk reach, characterized by the highest anabranching intensity (near Ponomarev island). It was significantly affected the change in sediment concentration throughout the 200 km reach of the Lena River under low water conditions. Figure 7 demonstrates the ΔW_R (kg s^{-1}) data obtained from two ADCP campaigns in 2020 and 2021. The corresponding blue dots in Figure 7 show similar trends revealed from satellite image SSC change. According to these measurements, both at low (8000 m^3s^{-1}) and average (15,000 m^3s^{-1}) flow conditions the erosion pattern dominated along the anabranching channel. ADCP data shows that the average increase in suspended sediment load was 4 kg s^{-1} (2% of the sediment discharge at the upper reach) and 6.4 kg s^{-1} (3% from the upper discharge) in the first case.

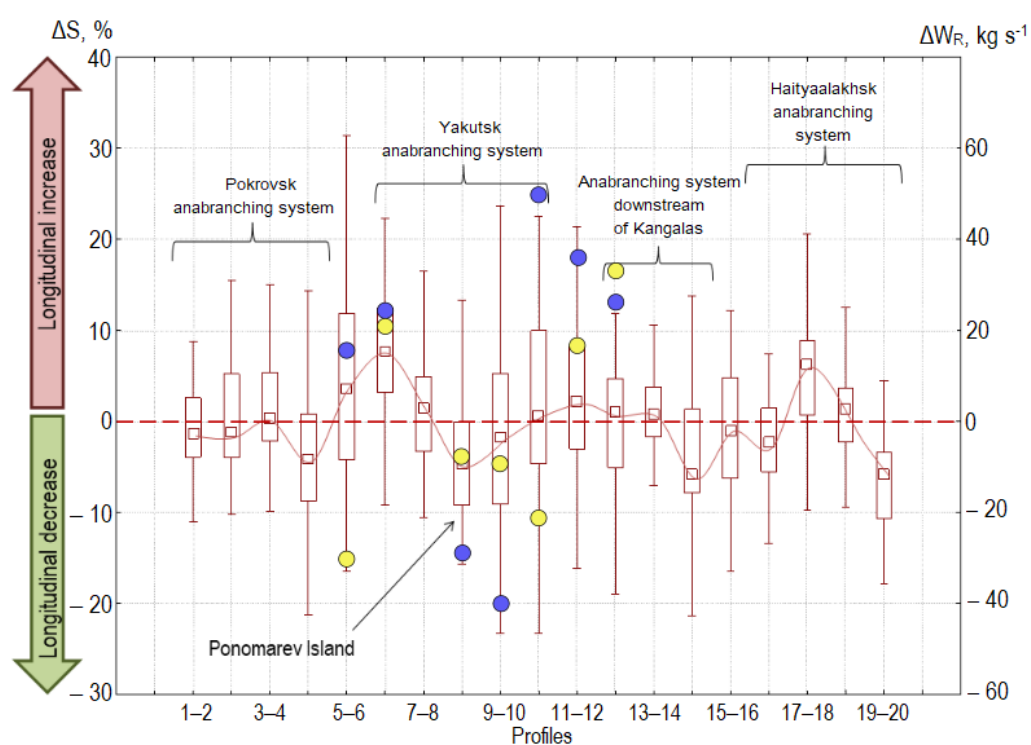


Figure 7. Longitudinal surface SSC changes (ΔS , %) and sediment load budget (ΔW_R , kg s^{-1}) in case study 1 of the Lena River (non-outlier range, mean, STD and 25–75%-interval) (profiles in Figure 2). Blue circles represent W_R values during the flood-water period, and yellow circles during low-water period.

We plotted the suspended sediment concentration changes for different intervals of water discharges: less than 10,000 m^3s^{-1} , from 10,000 m^3s^{-1} to 20,000 m^3s^{-1} and more than 20,000 m^3s^{-1} (Figure 8). Three discharges classes were identified based on their morphological effects. The water discharges ($< 10,000 m^3s^{-1}$) are related to conditions of low water observed during a significant part of the year and corresponds to the lowest hydraulic effects over the river channel. Bar-full discharge is observed here to the values higher than 20,000 m^3s^{-1} and relates to the level that submerges barren bars and the top of the water level before overbank submersion [16,17]. It lasts for about 30 days a year. When this water level reaches the base of the bank, thermal and fluvial erosion begins [16]. The SSC changes were calculated for groups of profiles: within the first anabranching channel near Pokrovsk (between profiles 1 and 3); in the anabranching channel near Yakutsk (between profiles 6 and 9), and within the Haityaalakhsksk anabranching channel (between profiles 16 and 19). Sedimentation patterns dominated during flood water (discharge more than

20,000 m³ s⁻¹), when ΔS decreased to -4% and varied from $+1$ to -9% at the confidence interval of 25–75%. The largest gradients of seasonal SSC variability are typical for the Yakutsk branching system. The rates of longitudinal increase in suspended sediment runoff were the highest ($\Delta S_0 = 6$ mg/L) in the upstream part of the middle reaches at the site of the flow distribution and formation of a complex of floodplain anabranches. In contrast, there was a decrease in the mean SSC in the branching system of the river near Ponomarev Island (on average for 62 situations) with a gradient between the profiles 8 and 9 ($\Delta S_0 = -3$ mg/L).

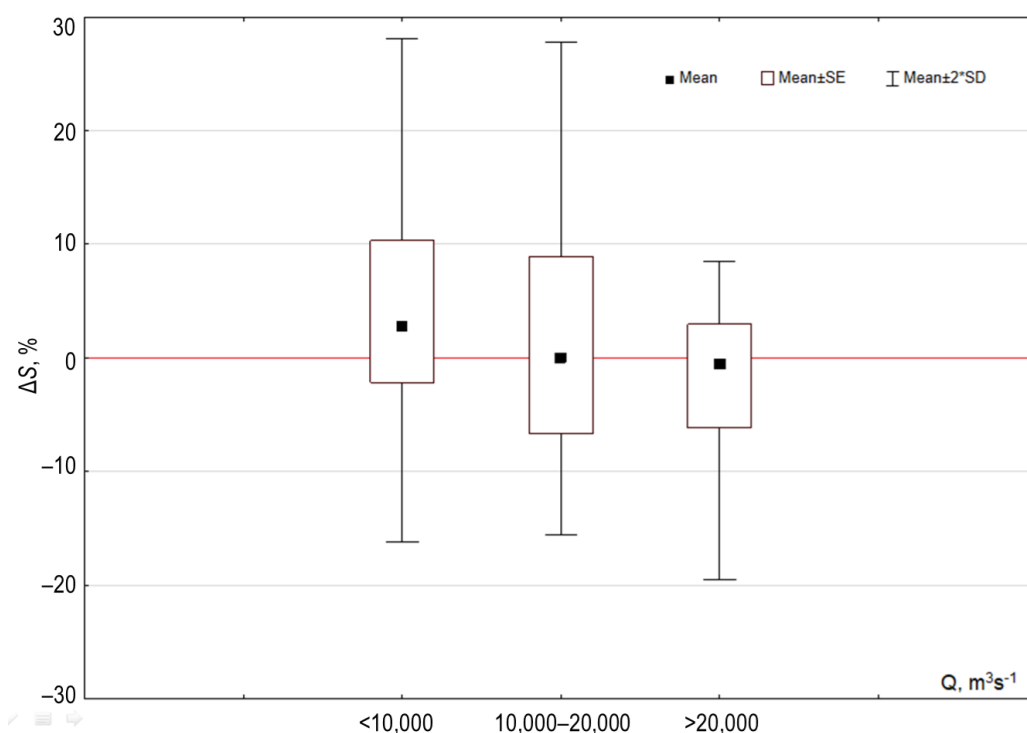


Figure 8. The surface SSC changes ΔS along case study 1 of the Lena River (62 situations in the period from 1992 to 2018).

4.3. Erosion and Sedimentation Patterns at the Lena River from Aldan to Zhigansk (Case Study 2)

Along case study 2, the sediment flow is driven by the inputs from the Aldan and Viluy Rivers. Here, the suspended sediments entering the merged river form plumes which can dominate SSC distribution during the peak and lower stages. Among the 30 analyzed Landsat images, 13 images had cross-sectional differences in SSC changes—an increase on the right bank of the Lena River (the influence of Aldan), 8 out of 30 images showed cross-sectional differences in SSC associated with a decreased SSC on the right bank (the influence of Lena). Nine images showed a uniform distribution of SSC in the studied area. Figure 9 provides two contrasting examples of such plumes related to the input of more turbid water from the Lena River (left) and the Aldan River (right). Due to the higher water discharge rate and larger sediment yield, the plumes from the Aldan dominate throughout the hydrological year.

The greatest differences in the SSC of the water flows in the cross-section of the river channel were observed at the beginning of the model section (first profile), closest to the confluence of the two rivers (Figure 9). Additionally, the decrease in the sediment differences with river cross-section was achieved 130–140 km from the Aldan and Lena confluences (profiles 11–12) where the river channel forms a relatively straight, narrow reach.

Downstream, 140 km below the Aldan confluence under the anabranching intensity increase the extended anabranching sector was associated with increased differences in the sediment concentration under left and right banks. This was also impacted by the Viluy River and smaller Lapiske River.

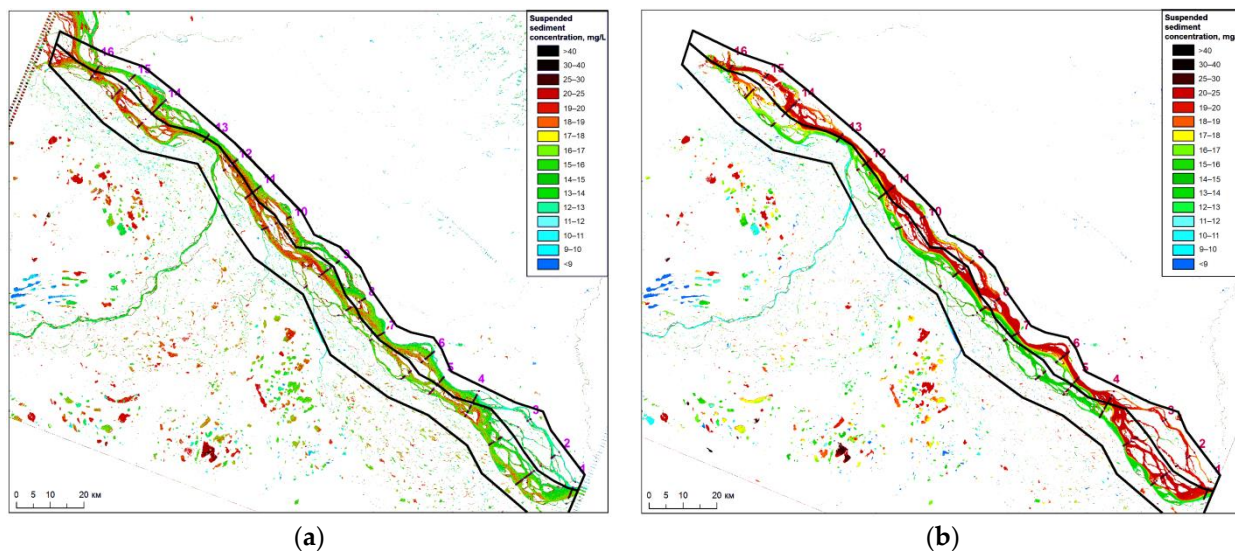


Figure 9. Examples of SSC maps along case study 2 demonstrating significant domination of the Lena River water discharge over the Aldan river (a)—28 August 2009, $Q_L/Q_A = 3.53$ ($Q_L = 17,700 \text{ m}^3\text{s}^{-1}$, $Q_A = 5,100 \text{ m}^3\text{s}^{-1}$), discharge ratio group—1) and domination of the Aldan River discharge over the Lena river (b)—31 August 2016, $Q_L/Q_A = 0.74$ ($Q_L = 13,200 \text{ m}^3\text{s}^{-1}$, $Q_A = 9,730 \text{ m}^3\text{s}^{-1}$), discharge ratio group—4).

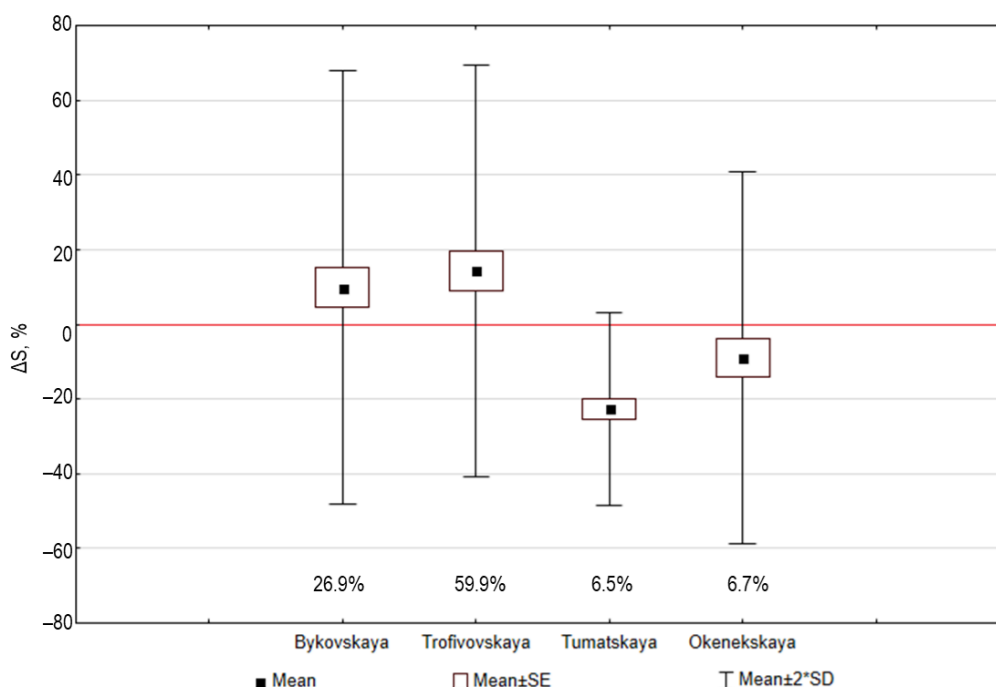
4.4. Erosion and Sedimentation Patterns at the Lena River Delta (Case Study 3)

We revealed contrasting patterns in the left and right sectors of the delta. The differences can be explained by the various sizes of the river channel (Table 6, Figure 10). A downward SSC increase was dominant in the Bykovskaya and Trofimovskaya branches which distributed over 86% of the total Lena discharge. Here, the downward increase of the surface sediment concentration (for example, from 45 mg/L in the main channel to 60 mg/L in the Trofimovskaya branch) occurred in 75% of the observed images. A significant drop in SSC was observed only within smaller distributaries, mostly Tumatskaya, which distributed less than 10% of the total Lena discharge. The average relative sediment change ΔS along the Tumatskaya branch was -22.7% and -8.96% along the Olenekskaya branch (a decrease in SSC from 16 mg/L in the main channel to 6 mg/L in the Olenekskaya channel). These channels were also characterized by the lowest slopes due to maximal channel length. Morphological expression of these phenomena is extended in sandy bars which are a dominant feature of both the Tumatskaya and Olenekskaya river channels. It is interesting to note that that SSC maps showed contrasting patterns under different hydrological conditions.

Table 6. Surface suspended sediment concentration changes along the main distributaries of the Lena delta.

Branch	% of The Total Discharge *	Average Channel Slope, m/km	ΔS_{mean}	ΔS_{max}	ΔS_{min}	Numbers of Analyzed Situations		
						$\Delta S > 0$	$\Delta S < 0$	In Total
Bykovskaya (right)	26.9	0.012	9.87	64.8	-57.6	17	11	28
Trofimovskaya (right)	59.9	0.011	14.4	72.6	-46.4	18	8	26
Tumatskaya (left)	6.5	0.009	-22.7	-2.65	-46.4	0	23	23
Olenekskaya (left)	6.7	0.008	-8.96	51.6	-49.7	6	16	22

*—measurements performed between 12–15 August 2022 with a total Lena discharge of 31,300 m³s⁻¹.

**Figure 10.** The suspended sediment changes ΔS (%) along the middle reach of the Lena River by relative discharges of the particular distributaries.

5. Discussion

5.1. Regional Empirical Models Validation

The proposed surrogate model enhanced capabilities of in situ monitoring of the Lena River. The observed models demonstrated specific relationships with sediment parameters. Regarding the turbidity units T (NTU), it was previously found that the increase in suspended matter size led to the growth of b coefficient which is the angle of the $SSC = f(T)$ graph [21]. A comparison of two sets of measurements at the Yakutsk anabranching system in September 2021 ($Q = 25,200 \text{ m}^3\text{s}^{-1}$) and June 2022 ($Q = 12,600 \text{ m}^3\text{s}^{-1}$) confirmed grain-size influence. Mean diameter (D_{50}) by September 2021 low-period measurements was 11.33 μm (a coefficient is 0.28) and the D_{50} value grew in the flood June 2022 period to 23.44 (the coefficient was 1.38). Even though we built a single relationship for different the hydrological conditions of the Lena River (Figure 4), some particular points on the relationship indicated that fine particles of weight m had a stronger influence on water

turbidity T , than the coarser particles of the same weight m . This indicates that the application of the model should be examined especially under extreme low-flow and high-water conditions. At the same time we noted that the proposed $SSC = f(T)$ relationship is similar to the coefficients observed in large plain alluvial rivers [48–50].

Among the set of models, the relationship $SSC = f(BI)$ was characterized by lowest R^2 values (Table 2). We attribute this to the fact that we used raw BI values, not corrected for intrinsic and ambient noise [51], as well as the impact of grain sizes on light backscattering. We compared linear fits between BI and SSC for sand fractions ($>50 \mu\text{m}$). Full suspended sediment concentration samples were reduced to macro class more than $50 \mu\text{m}$ in size, which represents the concentration of sand fraction in the river flow ($SSC > 50 \mu\text{m}$, mg/L). The results indicated that R^2 was increasing after changing SSC to $SSC > 50 \mu\text{m}$, from 0.59 to 0.67. These findings generally confirm previous research that a substantial correlation with corrected backscatter and SSC exists, while raw backscatter intensity does not reasonably predict SSC . Further research is recommended to proceed with corrected BI values and to estimate the error values for each of the individual ADCP units used in the study [38].

The obtained remote sensing models (Figure 5) were compared. The combination of regression model graphs for the Lena River in 2016, 2020 and 2022 reflects the influence of seasonal factors on the slope of regression equations lines. The type of model depends on changes in water discharges which explains the suspended sediment concentration, type, grain size, color and mineralogical composition of the sediments [43]. As the water discharges increased, the suspended sediment concentration and grain size also increased which influenced the spectral and optical water properties. As the grain size increased the radiance values decreased [52]. For example, the average size of sediments in integral samples according to the results of the 2016 expeditions was $96 \mu\text{m}$, and surface samples according to the results of the 2020 expeditions was $146 \mu\text{m}$. These factors led to a change in the slope of the regression equations lines.

5.2. Drivers of Sediment Budget along the Lena River

The contrasting erosion and sedimentation patterns were observed within the anabranching channel of the middle and lower Lena River which indicate that various drivers affect the sediment transport in different sections of the river. Along case study 1 the SSC drop along the river channel during high waters is explained by the inundation of vegetated islands and floodplains. During the high-water period, the surface sediment flows from the main channel towards the floodplain was detected through the increased number of river–floodplain connections as well as an increase in channel (water surface) width. For the analyzed images we counted the relative area of isolated floodplain lakes F_{lakes} and the total area of the surface waters along the anabranching channel $F_{channel}$. A positive relationship ($R^2 = 0.65$) was found between changes in suspended sediment concentrations ΔS and the ratio $F_{lakes}/F_{channel}$ which shows that the conditions of sediment concentration decline were associated with the decrease in river–floodplain connections. In particular, an increase in the $F_{lakes}/F_{channel}$ ratio corresponded to the water level drop over the Lena River during low-water season and further separation of particular floodplain water bodies (former branches of the river during high-water conditions) from the main channel. Higher $F_{lakes}/F_{channel}$ was related to a lower storage capacity due to the disconnectivity between the floodplain and the main channel. The role of the floodplain to attenuate surface runoff and capture sediment has been observed over largest anabranching rivers in the World (e.g., Amur, Mekong, Yangtze River) [6,53–55]. This floodplain flux can take a large portion of the total sediment flow of alluvial unconfined rivers during the high-water period, e.g., sediment from the main channel amounts to nearly 50% of the annual sediment flux entering the floodplain of the Amazon River [56]. Here, on the example of the Lena River we found that under low-water conditions the disconnectivity of the floodplain and the main channel led to transversal variability of SSC .

During low water, the increase in sediment concentration was associated with the intensification of riverbank erosion and sediment resuspension from the bottom to the upper layer along the riffle sections [13]. This was illustrated by the transport capacity (R_{tr}) which was counted according to the Rossinsky–Kuzmin equation [57] based on the ADCP velocity maps constructed for the case study 1 reach [11] as a function of water velocity (V) and channel depth (h) for each pixel of the Landsat-generated SSC map from 9 June 2016 (Lena discharge $12,400 \text{ m}^3\text{s}^{-1}$):

$$R_{tr} = 0.024 V^3/hu \quad (5)$$

where u is a settling velocity. Additionally, on the SSC map sediment concentration was averaged for 16 classes of velocity zones, delineated with an interval of 0.1 m s^{-1} . This yielded the significant equation ($R^2 = 0.91$) (Figure 11a):

$$SSC = 0.29 \ln(R_{tr}) + 11.5 \quad (6)$$

Considering the observed relationship between sediment concentration and suspended matter grain size (Figure 11b), we conclude that the hydrodynamics exert control over sediment sorting within the anabranching reach.

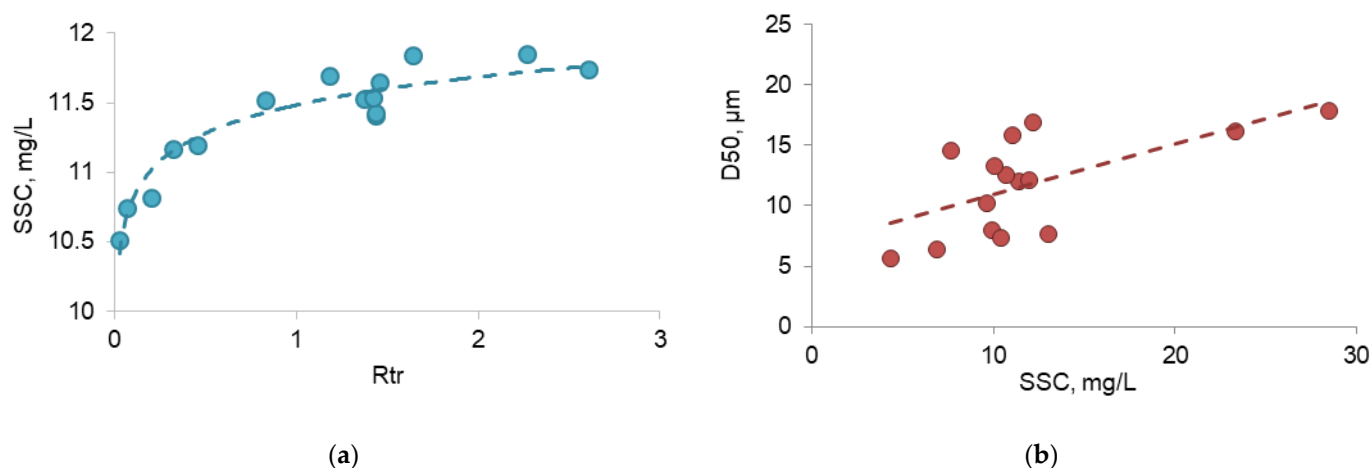


Figure 11. Relationship between the suspended sediment concentration (SSC) and (a) velocity (transport capacity— R_{tr}) from the measurements from 9 July 2016; (b)— mean sediment diameter (D_{50} , μm) from the measurement from 23 to 24 September 2021.

Due to the changes in velocity, the most significant influence on surface sediment concentration was from the small secondary branches which are a typical feature of anabranching channels. These branches can be relatively sinuous and extended over 10 km of the floodplain, separated by large islands (up to a few kilometers in width). Along case study 1 a significant drop in SSC was observed due to the dramatic increase in water discharge and water velocity. Here, both in the low- and peak-water period, the surface sediment flows from the main channel towards the secondary branches declined up to 50%, and in some case from 25 mg/L to 10 mg/L within rather short distances (less than 1 km) (Figure 6). Here, additionally, significant sediment sorting occurred. During the low-water period (by the data from 24 September 2021) in the 23 km, small left secondary branches of the Yakutsk anabranching system a decrease in SSC from 7.67 mg/L to 2.25 mg/L and mean diameter (D_{50}) from $10.9 \mu\text{m}$ to $6.54 \mu\text{m}$ occurred.

The drivers of the anabranching channel within case study 2 were related to the influence of the merging rivers. For statistical assessment we divided each profile into two parts, left-bank and right-bank, according to the geometric center of the anabranching channel (Figure 9) to analyze the effect the water flow on SSC changes. A significant difference in the SSC flow along the left and right banks of the Lena River was observed as a

function of the water discharges of the two rivers (Lena and Aldan). To perform this assessment, we compared SSC maps from 25 Landsat images with water discharges for gauges from two rivers—the Tabaga gauging station of the Lena River (Q_L) and Verkhoyansky Perevoz of the Aldan River (Q_A) (the subscripts L and A represent the Lena and Aldan Rivers, respectively). Further, the daily ratio Q_L/Q_A was calculated which ranged between 0.88 and 3.53 (Table 7). According to the rank, all cases were classified into four categories: (1) the Lena River water discharge significantly exceeds the Aldan River water discharge ($Q_L/Q_A > 1.75$), (2) the Lena River water discharge slightly exceeds the Aldan River water discharge ($1.25 < Q_L/Q_A < 1.75$), (3) similar water discharges in both rivers ($0.75 < Q_L/Q_A < 1.25$) and (4) the Aldan River water discharge slightly exceeds the Lena River water discharge ($Q_L/Q_A < 0.75$). Mean values of SSC were calculated for 16 profiles (Figure 2b) on the left S_l and right S_r segments of the river channel for each available satellite image. The Q_L/Q_A ratio was then compared with the S_l/S_r ratio. S_l/S_r changes along the Lena River case study 2 from the Lena and Aldan confluence (Figure 12) depicts that a greater difference in water discharges between the rivers was associated with higher sediment plumes along particular banks.

Table 7. The ratio of water discharge in the Lena River (Q_L) to the flow in the Aldan River (Q_A).

Satellite Image Date	Q_L , m^3s^{-1}	Q_A , m^3s^{-1}	Q_L/Q_A	Discharge Ratio Group	Satellite Image Date	Q_L , m^3s^{-1}	Q_A , m^3s^{-1}	Q_L/Q_A	Discharge Ratio Group
28 August 2009	17,700	5010	3.53	1	04 August 2006	6850	5760	1.19	3
30 August 2001	9500	4460	2.13	1	09 July 2014	11,700	10,400	1.13	3
30 September 2015	7620	3920	1.94	1	28 September 2000	9890	9180	1.08	3
03 September 2011	9590	5590	1.72	2	08 September 2007	8740	8220	1.06	3
12 June 2015	17,200	10,100	1.70	2	19 September 2011	10,800	10,300	1.05	3
02 August 2011	7880	4660	1.69	2	15 August 2016	12,900	13,100	0.98	3
14 June 2002	22,800	14,100	1.62	2	04 June 2013	20,700	22,000	0.94	3
01 August 2002	8770	5540	1.58	2	07 August 2013	22,800	26,000	0.88	3
12 June 2010	19,700	14,100	1.40	2	23 August 2013	15,900	18,400	0.86	3
12 June 2016	31,400	23,100	1.36	2	20 June 2013	18,200	21,600	0.84	3
10 September 1999	8650	6430	1.35	2	22 June 2013	14,100	18,800	0.75	4
08 June 2000	26,400	20,400	1.29	2	31 August 2016	9730	13,200	0.74	4
					10 June 2000	14,100	21,100	0.67	4

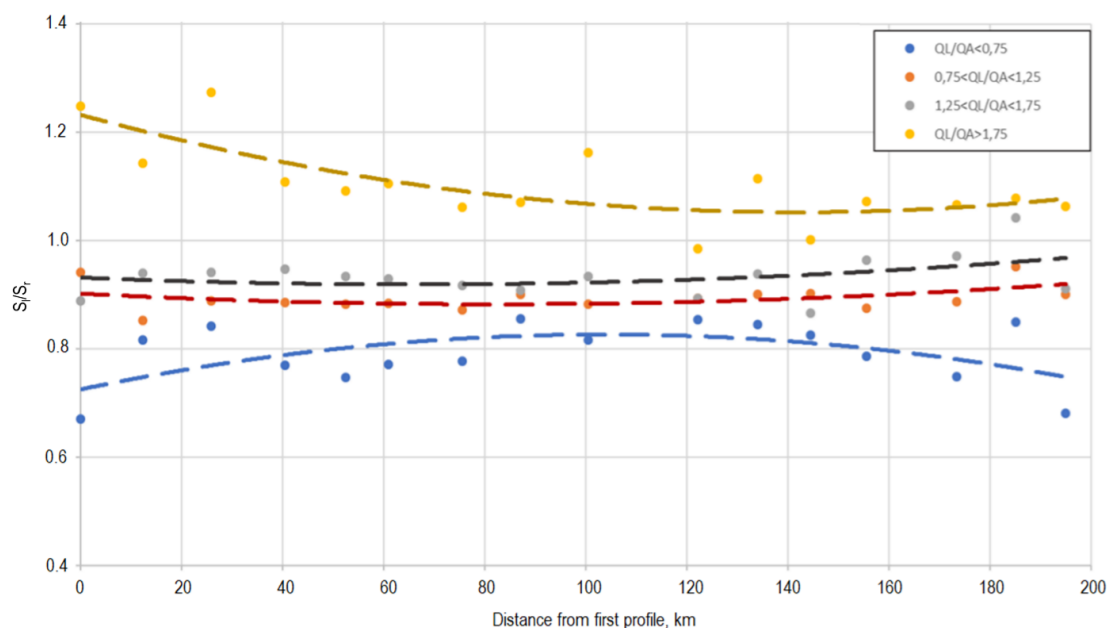


Figure 12. Changes in S_i/S_r ratio along the Aldan–Viluy reach of the Lena River under various hydrological conditions Q_L/Q_A .

Along case study 3, a downward increase in surface sediment concentration ($\Delta S > 0$) was associated with thermal erosion processes. The satellite images revealed a significant increase in sediment concentrations along the left bank. Despite the fact that bank retreat is governed by water discharge (duration and season) [16,17], we were unable to capture a significant relationship between sediment concentration changes and water flow rates. This may be explained by the non-linear links between water discharge, bank retreat and sediment concentration rates, e.g., for the middle Lena Gautier et al. [16] found a robust correlation between island morphological changes and several hydrologic parameters, including duration of bankfull discharges in May, the number of flood peaks in August; number of peaks; and number total peaks. These parameters were not used in our study which could lead to the conclusions related to the hydrological drivers of sedimentation and erosion patterns. At the same time, we found the relationships between average daily air temperature and bank erosion (SSC change). More specifically, average daily air temperature (according to the Tiksi weather station) was linked with the suspended sediment changes along the Bykovskaya and Trofimovskaya distributaries. This was seen especially in the range of air temperatures from 5 °C to 15 °C (Figure 13). The influence of a positive influx in total solar radiation and an increase in air temperatures contributes to the degradation of permafrost rocks and the activation of thermal erosion. Summer thawing and the associated activation of bank erosion raise sediment delivery into the hydrological network and further increase the concentration of solids in the river. Such effects are mostly marked along the left riverbanks of the southern exposure of the sublatitudinal sections of the Bykovskaya and Trofimovskaya channels.

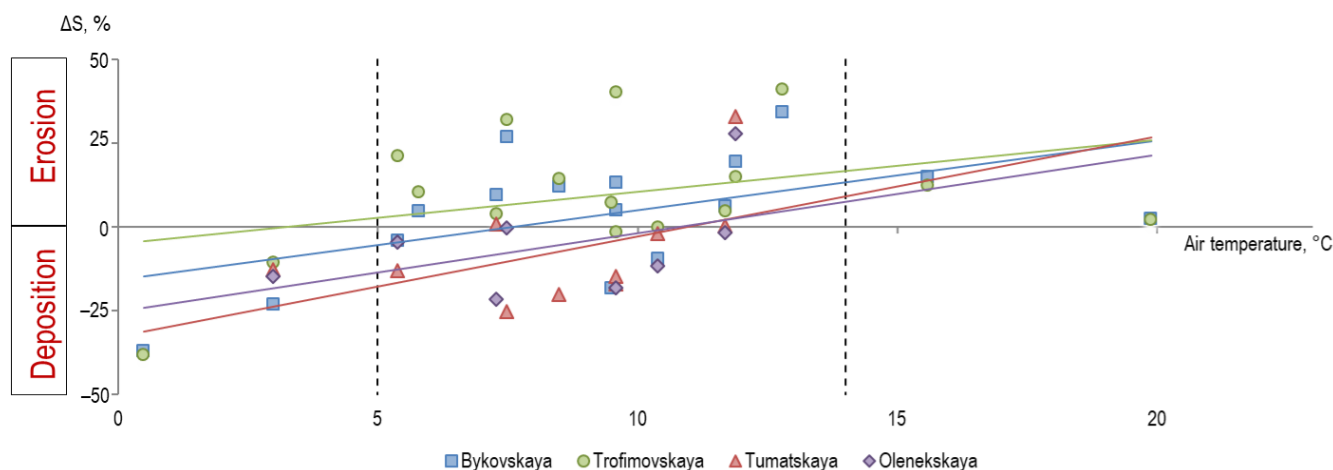


Figure 13. Relationship between the surface suspended sediment changes (ΔS) and air temperature ($^{\circ}\text{C}$) (Tiksi water station) in the Lena delta.

The obtained results imply a few important topics for further research and practice. They are useful for recalibrating the total export–discharge sediment models as far as the relationships between SSC and river discharge change owing to the shifting hydrological regimes and weather, thawing permafrost [58], and/or increasing terrestrial productivity. The obtained set of models (Table 2) can be used to develop large-scale and systematic hydrological monitoring systems in the Lena basin. Along the middle course, the more pronounced is the sediment exchanges between the channel systems and the floodplains which are important not just from a hydro-geomorphologic point of view, but also as a driver of sediment quality and geochemistry [59]. The results are critically important to our understanding of the Arctic carbon and nutrient cycles. Further, sediment-related research over the largest Arctic rivers can be combined with hydro-geochemical studies, also based on satellite-derived estimates already existing for Kolyma [60] and other large rivers [61]. The observed patterns have a few important and contrasting biogeochemical impacts on the riverine terrestrial flux of both mineral and organic components.

6. Conclusions

An effective combination of Landsat images with in situ measurements by gravimetric, turbidity and ADCP approaches were utilized to monitor the sediment transport along the anabranching channel along the middle and lower Lena River. Based on the set of empirical models, we revealed 3 transverse erosion and sedimentation patterns along the middle and lower Lena River anabranching channels

1. In the middle reach (case study 1) the anabranching channel was characterized by seasonal effects in erosion and sedimentation. Over 50% of the suspended load is trapped under peak flow conditions. A 10–20% increase in the suspended load occurred during low-flow conditions due to impacts of thermal erosion. Sediment traps along the anabranching channel exist within secondary branches ($100\text{--}200\text{ m}^3\text{s}^{-1}$). Sediment concentration changes due to variability of stream flow parameters (velocity). We found a significant relationship between the velocity (transport capacity) and sediment concentration and conclude that hydrodynamic controls sediment sorting within anabranching reach.
2. Anabranching channel reach which is influenced by the largest tributaries (Aldan and Viluy) (case study 2) is characterized by the sediment plumes which dominated spatial and temporal SSC distribution along the river section. A greater difference in water discharges between merging rivers is associated with higher sediment plumes along particular banks. Under these conditions, seasonal effects of sedimentation and erosion patterns cannot be detected.

3. The Lena delta (case study 3) demonstrates contrasting sediment patterns over its various parts. The observed changes in the suspended sediment transport in the delta are mostly related to channel erosion driven by thermal erosional processes. Here, the weather conditions during the summer affect the sediment budget along Yedoma banks which was reflected by the positive relationship observed between the daily air temperature and surface suspended sediment changes.

Author Contributions: Conceptualization, writing—original draft preparation, S.C.; methodology, validation, visualization, K.P. All authors have read and agreed to the published version of the manuscript.

Funding: Field works, study concept and numerical simulations are done within implementation of Russian Scientific Foundation project 21-17-00181. Additionally, study has been supported by the Kazan Federal University Strategic Academic Leadership Program ("PRIORITY-2030").

Institutional Review Board Statement: Not applicable.

Informed Consent Statement: Not applicable.

Data Availability Statement: Not applicable.

Acknowledgments: The Authors would like to thank the USGS for Landsat data, Russian Federal Service for Hydrometeorology and Environmental Monitoring (Roshydromet) and the Arctic Great Rivers Observatory (ArcticGRO) for the valuable measurement data.

Conflicts of Interest: The authors declare no conflict of interest.

References

1. Peterson, B.J.; Holmes, R.M.; McClelland, J.W.; Vörösmarty, C.J.; Lammers, R.B.; Shiklomanov, A.I.; Shiklomanov, I.A.; Rahmstorf, S. Increasing River Discharge to the Arctic Ocean. *Science* **2002**, *298*, 2171–2173. <https://doi.org/10.1126/science.1077445>.
2. Alexeevsky, N.I.; Chalov, R.S.; Berkovich, K.M.; Chalov, S.R. Channel changes in largest Russian rivers: Natural and anthropogenic effects. *Int. J. River Basin Manag.* **2013**, *11*, 175–191.
3. Chalov, S.R.; Liu, S.; Chalov, R.S.; Chalova, E.R.; Chernov, A.V.; Promakhova, E.V.; Berkovitch, K.M.; Chalova, A.S.; Zavadsky, A.S.; Mikhailova, N. Environmental and human impacts on sediment transport of the largest Asian rivers of Russia and China. *Environ. Earth Sci.* **2018**, *77*, 274. <https://doi.org/10.1007/s12665-018-7448-9>.
4. Escoube, R.; Rouxel, O.J.; Pokrovsky, O.S.; Schroth, A.; Max Holmes, R.; Donard, O.F.X. Iron isotope systematics in Arctic rivers. *Comptes Rendus -Geosci.* **2015**, *347*, 377–385. <https://doi.org/10.1016/j.crte.2015.04.005>.
5. Rachold, V.; Alabyan, A.M.; Hubberten, H.W.; Korotaev, V.N.; Zaitsev, A.A. Sediment transport to the Laptev Sea—Hydrology and geochemistry of the Lena River. *Polar Res.* **1996**, *15*, 183–196. <https://doi.org/10.3402/polar.v15i2.6646>.
6. Pietroni, J.; Nittrouer, J.A.; Chalov, S.R.; Dong, T.Y.; Kasimov, N.; Shinkareva, G.; Jarsjö, J. Sedimentation patterns in the Selenga River delta under changing hydroclimatic conditions. *Hydrol. Process.* **2018**, *32*, 278–292. <https://doi.org/10.1002/hyp.11414>.
7. Magritsky, D.V. *Annual Sediment Yield of Russian Arctic Rivers and Its Anthropogenic Changes*; Vestnik Moskovskogo Universiteta Series 5 Geography; Moskovskij Universitet: Moscow, Russia, 2010; pp. 17–24. (In Russian)
8. Hasholt, B.; Bobrovitskaya, N.; Bogen, J.; McNamara, J.; Mernild, S.H.; Milburn, D.; Walling, D.E. Sediment transport to the Arctic Ocean and adjoining cold oceans. *Hydrol. Res.* **2006**, *37*, 413–432.
9. Syvitski, J.P.M.; Kettner, A. Sediment flux and the anthropocene. *Philos. Trans. R. Soc. A Math. Phys. Eng. Sci.* **2011**, *369*, 957–975. <https://doi.org/10.1098/rsta.2010.0329>.
10. Gautier, E.; Costard, F. Anastomosing-fluvial systems in the periglacial zone: The Lena River and its main tributaries (Central Siberia). *Geogr. Phys. Quat.* **2000**, *54*, 327–342.
11. Golovlyov, P.; Kornilova, E.; Krylenko, I.; Belikov, V.; Zavadskii, A.; Fingert, E.; Borisova, N.; Morozova, E. Numerical modeling and forecast of channel changes on the river Lena near city Yakutsk. *Proc. Int. Assoc. Hydrol. Sci.* **2019**, *381*, 65–71. <https://doi.org/10.5194/piahs-381-65-2019>. (In Russian)
12. Bolshiyarov, D.Y.; Makarov, A.S.; Schneider, V.; Stoof, G. *Origin and Development of the Lena River Delta*; AARI: St. Petersburg, Russia, 2013. (In Russian)
13. Chalov, S.; Prokopeva, K.; Habel, M. North to South Variations in the Suspended Sediment Transport Budget within Large Siberian River Deltas Revealed by Remote Sensing Data. *Remote Sens.* **2021**, *13*, 4549. <https://doi.org/10.3390/rs13224549>.
14. Fedorova, I.; Chetverova, A.; Bolshiyarov, D.; Makarov, A.; Boike, J.; Heim, B.; Morgenstern, A.; Overduin, P.P.; Wegner, C.; Kashina, V.; et al. Lena Delta hydrology and geochemistry: Long-term hydrological data and recent field observations. *Biogeosciences* **2015**, *12*, 345–363. <https://doi.org/10.5194/bg-12-345-2015>.

15. Agafonova, S.A.; Frolova, N.A.; Surkova, G.V.; Koltermann, K.P. Modern characteristics of the ice regime of Russian arctic rivers and their possible changes in the 21st century. *Geogr. Environ. Sustain.* **2017**, *10*, 4–15. <https://doi.org/10.24057/2071-9388-2017-10-4-4-15>.
16. Georgiadi, A.G.; Koronkevich, N.I.; Milyukova, I.P.; Barabanova, E.A. Integrated projection for runoff changes in large Russian river basins in the XXI century. *Geogr. Environ. Sustain.* **2016**, *9*, 38–46. <https://doi.org/10.24057/2071-9388-2016-9-2-59-65>.
17. Lammers, R.B.; Shiklomanov, A.I.; Vörösmarty, C.J.; Fekete, B.M.; Peterson, B.J. Assessment of contemporary Arctic river runoff based on observational discharge records. *J. Geophys. Res. Atmos.* **2001**, *106*, 3321–3334. <https://doi.org/10.1029/2000JD900444>.
18. Costard, F.; Gautier, E.; Brunstein, D.; Hammadi, J.; Fedorov, A.; Yang, D.; Dupeyrat, L. Impact of the global warming on the fluvial thermal erosion over the Lena River in Central Siberia. *Geophys. Res. Lett.* **2007**, *34*, L14501. <https://doi.org/10.1029/2007GL030212>.
19. Gautier, E.; Dépret, T.; Caverio, J.; Costard, F.; Vermoux, C.; Fedorov, A.; Konstantinov, P.; Jammet, M.; Brunstein, D. Fifty-year dynamics of the Lena River islands (Russia): Spatio-temporal pattern of large periglacial anabranching river and influence of climate change. *Sci. Total Environ.* **2021**, *783*, 147020. <https://doi.org/10.1016/j.scitotenv.2021.147020>.
20. Tananaev, N.I. Hydrological and sedimentary controls over fluvial thermal erosion, the Lena River, central Yakutia. *Geomorphology* **2016**, *253*, 524–533. <https://doi.org/10.1016/j.geomorph.2015.11.009>.
21. Chalov, S.; Golosov, V.; Tsyplenkov, A.; Theuring, P.; Zakerinejad, R.; Märker, M.; Samokhin, M. A toolbox for sediment budget research in small catchments. *Geogr. Environ. Sustain.* **2017**, *10*, 43–68. <https://doi.org/10.24057/2071-9388-2017-10-4-43-68>.
22. Chalov, S.R.; Bazilova, V.O.; Tarasov, M.K. Suspended sediment balance in Selenga delta at the late XX–early XXI century: Simulation by LANDSAT satellite images. *Water Resour.* **2017**, *44*, 463–470. <https://doi.org/10.1134/S0097807817030071>.
23. Pavelsky, T.M.; Smith, L.C. Remote sensing of suspended sediment concentration, flow velocity, and lake recharge in the Peace-Athabasca Delta, Canada. *Water Resour. Res.* **2009**, *45*, W11417. <https://doi.org/10.1029/2008WR007424>.
24. Martinez, J.M.; Guyot, J.L.; Filizola, N.; Sondag, F. Increase in suspended sediment discharge of the Amazon River assessed by monitoring network and satellite data. *Catena* **2009**, *79*, 257–264. <https://doi.org/10.1016/j.catena.2009.05.011>.
25. Wang, J.; Lu, X.; Zhou, Y. Retrieval of suspended sediment concentrations in the turbid water of the Upper Yangtze River using Landsat ETM+. *Chin. Sci. Bull.* **2007**, *52*, 273–280. <https://doi.org/10.1007/s11434-007-7012-6>.
26. Park, E.; Latrubesse, E.M. Modeling suspended sediment distribution patterns of the Amazon River using MODIS data. *Remote Sens. Environ.* **2014**, *147*, 232–242. <https://doi.org/10.1016/j.rse.2014.03.013>.
27. Park, E.; Latrubesse, E.M. A geomorphological assessment of wash-load sediment fluxes and floodplain sediment sinks along the lower Amazon River. *Geology* **2019**, *47*, 403–406. <https://doi.org/10.1130/G45769.1>.
28. Latrubesse, E.M.; Park, E.; Kastner, K. The Ayeyarwady River (Myanmar): Washload transport and its global role among rivers in the Anthropocene. *PLoS ONE* **2021**, *16*, e0251156. <https://doi.org/10.1371/journal.pone.0251156>.
29. Mertes, L.A.K.; Smith, M.O.; Adams, J.B. Estimating suspended sediment concentrations in surface waters of the Amazon River wetlands from Landsat images. *Remote Sens. Environ.* **1993**, *43*, 281–301. [https://doi.org/10.1016/0034-4257\(93\)90071-5](https://doi.org/10.1016/0034-4257(93)90071-5).
30. Yang, D.; Kane, D.L.; Hinzman, L.D.; Zhang, X.; Zhang, T.; Ye, H. Siberian Lena River hydrologic regime and recent change. *J. Geophys. Res. Atmos.* **2002**, *107*, 4694. <https://doi.org/10.1029/2002JD002542>.
31. Babin, M.; Stramski, D.; Ferrari, G.M.; Claustre, H.; Bricaud, A.; Obolensky, G.; Hoepffner, N. Variations in the light absorption coefficients of phytoplankton, nonalgal particles, and dissolved organic matter in coastal waters around Europe. *J. Geophys. Res. Ocean.* **2003**, *108*. <https://doi.org/10.1029/2001jc000882>.
32. Strauss, J.; Laboor, S.; Schirrmeister, L.; Fedorov, A.N.; Fortier, D.; Froese, D.; Fuchs, M.; Günther, F.; Grigoriev, M.; Harden, J.; et al. Circum-Arctic Map of the Yedoma Permafrost Domain. *Front. Earth Sci.* **2021**, *9*, 758360. <https://doi.org/10.3389/feart.2021.758360>.
33. Tananaev, N.I. Seasonal and long-term freezing of the cryolithozone river beds and its influence on channel changes (on the example of average Lena). *Eros. Fluv. Process. Hydroecol. Probl.* **2004**, 195–201. (In Russian)
34. Chalov, R.S. *Fluvial Processes: Theory and Applications*; Springer International Publishing: Cham, Switzerland, 2021; ISBN 978-3-030-66182-3.
35. Schwamborn, G.; Rachold, V.; Grigoriev, M.N. Late Quaternary sedimentation history of the Lena Delta. *Quat. Int.* **2002**, *89*, 119–134. [https://doi.org/10.1016/S1040-6182\(01\)00084-2](https://doi.org/10.1016/S1040-6182(01)00084-2).
36. Latrubesse, E.M. Patterns of anabranching channels: The ultimate end-member adjustment of mega rivers. *Geomorphology* **2008**, *101*, 130–145. <https://doi.org/10.1016/j.geomorph.2008.05.035>.
37. Ivanov, V.V.; Piskun, A.A.; Korabel, R.A. Distribution of Runoff through the Main Channels of the Lena River Delta. *Proc. AARI* **1983**, *378*, 59–71. (In Russian)
38. Chalov, S.; Moreido, V.; Ivanov, V.; Chalova, A. Assessing suspended sediment fluxes with acoustic Doppler current profilers: Case study from large rivers in Russia. *Big Earth Data* **2022**, 1–23. <https://doi.org/10.1080/20964471.2022.2116834>.
39. Dominguez Ruben, L.G.; Szupiany, R.N.; Latosinski, F.G.; López Weibel, C.; Wood, M.; Boldt, J. Acoustic Sediment Estimation Toolbox (ASET): A software package for calibrating and processing TRDI ADCP data to compute suspended-sediment transport in sandy rivers. *Comput. Geosci.* **2020**, *140*, 104499. <https://doi.org/10.1016/j.cageo.2020.104499>.
40. Carlson, P.R.; Conomos, T.J.; Janda, R.J.; Peterson, D.H. *Principal Sources and Dispersal Patterns of Suspended Particulate Matter in Nearshore Surface Waters of the Northeast Pacific Ocean*; Final Report; EROS Center: Sioux Falls, SD, USA, 1974.
41. Curran, P.J.; Novo, E.M.M. The relationship between suspended sediment concentration and remotely sensed spectral radiance. *Rev. J. Coast. Res.* **1988**, 361–368.

42. Wackerman, C.; Hayden, A.; Jonik, J. Deriving spatial and temporal context for point measurements of suspended-sediment concentration using remote-sensing imagery in the Mekong Delta. *Cont. Shelf Res.* **2017**, *147*, 231–245. <https://doi.org/10.1016/j.csr.2017.08.007>.
43. Novo, E.M.M.; Hansom, J.D.; Curran, P.J. The effect of sediment type on the relationship between reflectance and suspended sediment concentration. *Int. J. Remote Sens.* **1989**, *10*, 1283–1289. <https://doi.org/10.1080/01431168908903967>.
44. Chavez, P.S. Image-Based Atmospheric Corrections—Revisited and Improved. *Photogramm. Eng. Remote Sens.* **1996**, *62*, 1025–1036.
45. Chavez, P.S. Radiometric calibration of Landsat Thematic Mapper multispectral images. *Photogramm. Eng. Remote Sens.* **1989**, *55*, 1285–1294.
46. Chander, G.; Markham, B.L.; Helder, D.L. Summary of current radiometric calibration coefficients for Landsat MSS, TM, ETM+, and EO-1 ALI sensors. *Remote Sens. Environ.* **2009**, *113*, 893–903. <https://doi.org/10.1016/j.rse.2009.01.007>.
47. Chavez, P.S. An improved dark-object subtraction technique for atmospheric scattering correction of multispectral data. *Remote Sens. Environ.* **1988**, *24*, 459–479. [https://doi.org/10.1016/0034-4257\(88\)90019-3](https://doi.org/10.1016/0034-4257(88)90019-3).
48. Sokolov, D.I.; Erina, O.N.; Tereshina, M.A.; Puklakov, V.V. Impact of Mozhaysk Dam on the Moscow River Sediment Transport. *Geogr. Environ. Sustain.* **2020**, *13*, 24–31. <https://doi.org/10.24057/2071-9388-2019-150>.
49. Ankcorn, P.D. Clarifying Turbidity—The Potential and Limitations of Turbidity as a Surrogate for Water-Quality Monitoring. In Proceedings of the 2003 Georgia Water Resources Conference, Tifton, GA, USA, 23–24 April 2003.
50. Belozeroва, E. V.; Chalov, S.R. *Assessment of River Water Turbidity Using the Optic Methods*; Vestnik Moskovskogo Universiteta Seriya 5 Geografiya; Moskovskij Universitet: Moscow, Russia, 2013; pp. 39–45. (In Russian)
51. Szupiany, R.N.; Lopez Weibel, C.; Guerrero, M.; Latosinski, F.; Wood, M.; Dominguez Ruben, L.; Oberg, K. Estimating sand concentrations using ADCP-based acoustic inversion in a large fluvial system characterized by bi-modal suspended-sediment distributions. *Earth Surf. Process. Landf.* **2019**, *44*, 1295–1308. <https://doi.org/10.1002/esp.4572>.
52. Choubey, V.K. Laboratory experiment, field and remotely sensed data analysis for the assessment of suspended solids concentration and secchi depth of the reservoir surface water. *Int. J. Remote Sens.* **1998**, *19*, 3349–3360. <https://doi.org/10.1080/014311698214037>.
53. Binh, D. Van; Kantoush, S.; Sumi, T. Changes to long-term discharge and sediment loads in the Vietnamese Mekong Delta caused by upstream dams. *Geomorphology* **2020**, *353*, 107011. <https://doi.org/10.1016/j.geomorph.2019.107011>.
54. Martynov, A.V. Influence Of The Large Flood on the Element Composition of Fluvisols in the Amur River Valley. *Geogr. Environ. Sustain.* **2020**, *13*, 52–64. <https://doi.org/10.24057/2071-9388-2019-03>.
55. Wang, J.J.; Lu, X.X.; Liew, S.C.; Zhou, Y. Retrieval of suspended sediment concentrations in large turbid rivers using Landsat ETM+: An example from the Yangtze River, China. *Earth Surf. Process. Landf.* **2009**, *34*, 1082–1092. <https://doi.org/10.1002/esp.1795>.
56. Bonnet, M.P.; Barroux, G.; Martinez, J.M.; Seyler, F.; Moreira-Turcq, P.; Cochonneau, G.; Melack, J.M.; Boaventura, G.; Maurice-Bourgoin, L.; León, J.G.; et al. Floodplain hydrology in an Amazon floodplain lake (Lago Grande de Curuaí). *J. Hydrol.* **2008**, *349*, 18–30. <https://doi.org/10.1016/j.jhydrol.2007.10.055>.
57. Chalov, S.R.; Alexeevsky, N.I. Braided rivers: Structure, types and hydrological effects. *Hydrol. Res.* **2015**, *46*, 258. <https://doi.org/10.2166/nh.2013.023>.
58. Vandenberghe, J. Climate forcing of fluvial system development: An evolution of ideas. *Quat. Sci. Rev.* **2003**, *22*, 2053–2060. [https://doi.org/10.1016/S0277-3791\(03\)00213-0](https://doi.org/10.1016/S0277-3791(03)00213-0).
59. Gordeev, V.V.; Rachold, V.; Vlasova, I.E. Geochemical behaviour of major and trace elements in suspended particulate material of the Irtysh river, the main tributary of the Ob river, Siberia. *Appl. Geochem.* **2004**, *19*, 593–610. <https://doi.org/10.1016/j.apgeochem.2003.08.004>.
60. Griffin, C.G.; Frey, K.E.; Rogan, J.; Holmes, R.M. Spatial and interannual variability of dissolved organic matter in the Kolyma River, East Siberia, observed using satellite imagery. *J. Geophys. Res.* **2011**, *116*, G03018. <https://doi.org/10.1029/2010JG001634>.
61. McClelland, J.W.; Holmes, R.M.; Peterson, B.J.; Raymond, P.A.; Striegl, R.G.; Zhulidov, A.V.; Zimov, S.A.; Zimov, N.; Tank, S.E.; Spencer, R.G.M.; et al. Particulate organic carbon and nitrogen export from major Arctic rivers. *Glob. Biogeochem. Cycles* **2016**, *30*, 629–643. <https://doi.org/10.1002/2015GB005351>.